J. Fluid Mech. (1994), *vol.* 281, *pp.* 319–356

Observations of polymer conformation during flow through a fixed fibre bed

By ANTHONY R. EVANS[1], ERIC S. G. SHAQFEH[1] AND PAUL L. FRATTINI[2]

[1]Department of Chemical Engineering, Stanford University, Stanford, CA 94305, USA

[2]Eifle Inc., c/o 11465 Clayton Road, San Jose, CA 95127, USA

(Received 3 August 1993 and in revised form 29 June 1994)

Linear birefringence measurements of dilute and semi-dilute polyisobutylene solutions following flow through a disordered fixed fibre bed of 2.47% solids volume fraction provide both transient and steady measurements of chain deformation. Our results indicate that the flexible polyisobutylene polymers undergo a large conformation change, stretching in the direction of the average flow. This occurs even though the average flow in the bed is a plug flow which would not cause any polymer stretch by itself. The polymer stretch or conformation change increases with the number of chain interactions with bed fibres and ultimately reaches a steady-state value that can be correlated with the pore-size Deborah number (i.e. a characteristic polymer relaxation time divided by a characteristic flow time in the bed pore). Large changes in the polymer conformation are noted for values of the Deborah number, $De > 5$. In addition, the time to steady state scales with the characteristic flow time within a pore over a large range of Deborah numbers. The pressure drop across the fibre bed was also measured simultaneously with the birefringence measurement and was found to be directly proportional to the birefringence throughout the range of De investigated. Thus, we show empirically, for the first time, that chain elongation, which produces normal stress anisotropy within the fluid, is directly responsible for the increased flow resistance. These findings are then analysed in the light of recent theories for the response of polymer molecules in fixed bed flow fields (Shaqfeh & Koch 1992). It is shown that our results are consistent with the interpretation that these flows are stochastic strong flows, which create an apparent 'coil-stretch' transition. After extending the theory of Shaqfeh & Koch to account for the specifics in the experiments, including the bed geometry and statistics as well as the polydispersity of the polymer solutions, it is shown that the theory can predict most of the experimental results both qualitatively and quantitatively.

1. Introduction

The behaviour of polymer molecules in porous media flows has been extensively examined during the last three decades (Marshall & Metzner 1967; James & McLaren 1975; Durst, Haas & Kaczmar 1981). Early studies reported that dilute polymer solutions subjected to flow through fixed porous media exhibited apparent strain-thickening rheological behaviour. Specifically, the pressure drop necessary to pump the fluid at a constant flow rate increased dramatically with the presence of polymeric material even though the concentration of the high molecular weight species was as low as 6 p.p.m. Early among these studies was the work of James & McLaren (1975), who reported not only the increase in flow resistance present in the polymeric flow through

fixed beds of glass spheres, but also evidence of polymer degradation in the flow. This work and the supplementary studies of Durst *et al.* (1981) led to the supposition that flow resistance was increasing because the polymers were undergoing a type of 'coil-stretch' conformation change similar to that experienced by flexible polymer chains in a rheological strong flow (Olbricht, Rallison & Leal 1982; Tanner 1985). Note that this apparent transition occurred even though the average flow in a porous bed is a plug flow, and thus there are no average velocity gradients within the bed to alter polymer conformation.

These early studies are characterized by several key features. First, the porous beds consisted almost exclusively of packed geometries in which the solids volume fraction was large and the bed geometries could at best only be inferred from likely packing geometries. Thus, the solids volume fraction was the main feature characterizing the bed. Secondly, the primary observable was a measurement of the pressure drop across the bed. Thus, conclusions about the average polymer conformation could only be inferred from these pressure measurements and remained qualitative.

The purpose of the present communication is two-fold. First, we wish to present a complete set of experimental measurements directly probing polymer conformation change in flow through porous media. The second goal is to analyse the results in the light of existing theories of stochastic flows, thus comparing predicted conformation change to the measured values.

The experimental work we present differs in two ways from previous experiments. First, in §2 we describe the unique porous bed considered. It is a dilute (2.47%) fibre bed that is statistically well-characterized but disordered. Since the bed is dilute, there exist no geometric or steric effects which align and stretch the polymers. In addition, the probability of a polymer passing to within a fibre radius from a given fibre is small, since the Darcy pore size in the dilute media is much larger than the characteristic scale (i.e. the fibre radius) of the constituent bed particles. Therefore, the leading effect for small bed volume fraction is expected to be due to the far-field hydrodynamic interactions (those that scale on the pore size) between the bed particles and the polymers.

Secondly, rather than relying entirely on pressure drop measurements to infer polymer conformation, in addition we measure the flow birefringence, a method which directly measures polymer conformation change (Frattini & Fuller, 1984; Galante 1991). Birefringence measurements on flexible chain polymer systems have been used as a means of experimentally investigating flow-induced microstructure deformation for many years (Kuhn & Grun 1942; Coleman, Dill & Toupin 1970; Peterlin 1976; Wales 1976; Janeschitz-Kreigl 1983; DuPuis, Layec & Wolff, 1986; Larson, Kahn & Raju 1988; McHugh, Mackay & Khomami 1988; Pearson *et al.* 1989; Geffroy & Leal 1990; Fuller 1990; Galante & Frattini 1993; Kishbaugh & McHugh 1993). We have used a similar technique – conservative linear dichroism – in our previous study of rigid particle orientation in flow through the same fixed bed (Frattini *et al.* 1991).

In §2 we describe the polarization modulation technique utilized to measure the birefringence of the polymer solution exiting the fibre bed. This method offers a direct non-invasive probe of polymer conformation, and thus is a substantial improvement over previous experiments. Furthermore, the measurement of birefringence at the bed exit facilitates analysis of polymer conformation averaged over the cross-sectional area of the laser beam as opposed to an average over the larger length typical in pressure drop measurements.

The polymer solutions, including practical aspects of their preparation, are also discussed in §2. The polymer solutions analysed were similar in composition to the

three-component Boger fluid, M1 (Sridhar 1990; Nguyen & Sridhar 1990). The polymer of interest was a high-molecular-weight polyisobutylene (PIB) in solution with a low-molecular-weight polybutene (PB), the latter serving as a viscosifier to increase the characteristic relaxation time of the solvated polymer. In addition, we used a volatile solvent, trichloroethylene, to initially solvate the PIB. Like M1, this solution exhibited a constant shear viscosity over a large range of shear rates (0.1 s^{-1}–50 s^{-1}) and the PIB was relatively polydisperse. However, unlike M1 the concentration of the PIB in solution was restricted to the dilute and near dilute regime (50, 100, 333 and 1000 p.p.m.).

In §3 both transient and steady-state results are presented. We show, via measurements of the solution birefringence, that flow through a dilute fibre bed produces a high degree of polymer stretch in the direction of the mean velocity. The pressure drop across the bed was found to track the birefringence, indicating that the apparent hydrodynamic resistance of the bed increases as chains deform. The polymers, on average, become increasingly stretched from the coiled equilibrium state as they flow through the fixed fibre bed, and the degree of this average stretch can be correlated with the *distance* traversed through the bed by a polymer. The magnitude of stretch eventually attains a steady-state value which increases monotonically with the pore-size Deborah number ($De = U\lambda/\kappa^{1/2}$, where U is the mean flow velocity, λ is the characteristic relaxation time of the polymer, and $\kappa^{1/2}$ is the pore size of the bed). It is shown that the degree of stretch at steady state increases significantly above a certain value of the pore-size Deborah number ($De \sim 5$) while relatively little stretch is noted at pore-size Deborah numbers lower than this value.

We note that the ability of the pore-size Deborah number to determine the onset of significant polymer stretch suggests that this stretch is due to the interactions of the polymers with the far-field velocity gradient fluctuations (which scale on the pore size) rather than 'close' hydrodynamic interactions which are determined by the geometry of individual bed fibres (such as stretch due to the rear end stagnation point (Harlen, Hinch & Rallison 1992)).

The degree of stretch at steady state is shown to be large through evidence of permanent polymer degradation, measurements of a large pressure drop across the bed, and comparison of our results with birefringence data obtained in the extensional flow of a two-roll mill (a known strong flow) for a similar polymer system (Geffroy & Leal 1990). We show that the magnitude of the steady-state values for both systems are of the same order of magnitude. Unlike Geffroy & Leal (1990) who see chain scission, other authors have subjected flexible systems to extensional flows in opposing jet-type geometries and have concluded that one explanation of their light scattering data might be that intrachain segments orient but the chain itself is not fully elongated (Cathey & Fuller 1990; Menasveta & Hoagland 1991). However, the large pressure drops seen in our dilute fibre bed in conjunction with our observation that there exists a direct proportionality between the pressure drop and the birefringence demonstrates that the increased bed resistance is indeed due to the elastic stresses which develop as the chain is fully elongated, and that the scission we also observe is occurring in highly elongated chains.

Finally, our experimental results show a dilute concentration regime, where polymer–polymer interactions are negligible. This is determined through examination of the flows of fluids at four polymer concentrations (50, 100, 333, 1000 p.p.m.). The 50 and 100 p.p.m. solutions behave as dilute solutions for all Deborah numbers examined. However, the transition concentration from dilute to semi-dilute is found to be conformation dependent.

The results in §3 are then analysed in the light of the existing theory for the flow of polymer solutions through dilute fibre beds, but modified to include the specific characteristics of our experimental system. In short, previous theoretical studies have involved as examination of the behaviour of model polymer molecules (usually dumbbell models) in their flow through simple deterministic geometries designed, in principle, to capture the salient characteristics of porous media or fixed bed flows. The most oft-used model is the wavy-walled tube (Deiber & Schowalter 1979; Zick & Homsy 1984; Pilitsis & Beris 1989). These studies range from the use of analytical techniques (e.g. perturbation theory) to large computational studies which include full numerical solutions of the flow of model elastic fluids (i.e. Oldroyd-B fluids) in wavy-walled tubes. All of these studies failed to show the large degree of 'global' polymer stretch suggested by previous experimental work.

In more recent work, numerical solutions of the flow of model elastic solutions past single cylinders or periodic arrays of cylinders have been presented by Townsend (1989); Chilcott & Rallison (1988); Chmielewski, Petty & Jayaraman (1990); Skartsis, Khomami & Kardos (1992); and McKinley, Armstrong & Brown (1993). Chilcott & Rallison (1988), looking at flow past a single cylinder, showed that the rear stagnation point in the flow past fixed cylinders does produce a region of highly stretched polymers. Chmielewski *et al.* (1990), who studied arrays of cylinders for a number of geometries, determined that polymer stretch not only occurred near the rear stagnation point but could also occur in the gaps between the cylinders owing to the interparticle interactions. Although these studies show large polymer stretch locally, they fail to produce the large polymer stretch considered necessary to obtain large flow resistance when *averaged* over the entire polymer population. In other words, while some polymers become highly stretched in regions where close interactions are an important mechanism for stretch, the majority of polymers will not enter these extensional areas. Thus, *on average*, the polymers will not be in a highly stretched state. Skartsis *et al.* (1992) used an 'improved capillary' model to describe the flow past cylindrical arrays which, although yielding improved predictions when compared to *idealized* porous arrays, was unable to predict the high pressure drops encountered in disordered beds.

In a different approach, Shaqfeh & Koch (1992) argued that the disorder in fixed beds was a crucial element lacking in all of the previous theoretical models. They used the method of averaged equations (Hinch 1977) to develop an ensemble-averaged description of the dynamics of Hookean and FENE dumbbells (Bird *et al.* 1978) flowing through disordered dilute fixed beds of spheres or fibres. Their kinetic theory showed that, for dilute fixed media, the largest contribution to the evolution of the configuration of flowing dumbbells came from long-range interactions, i.e. hydrodynamic interactions on the scale of the pore size in the media. The pore sizes in these dilute media are much larger than the characteristic scale of the constituent particles in the media, hence the name 'long-range' interactions. The solution of the evolution equation which included these long-range interactions showed a dramatic increase in the radius of gyration at a specific critical flow rate which was very similar to the 'coil-stretch' transition that is predicted in classical strong flows. However, unlike traditional 'coil-stretch' flows, the transition of the polymers to a highly stretched conformation comes about by multiple diffusive hydrodynamic interactions with the bed particles. In addition, the critical flow rate or, in dimensionless terms, the critical pore-size Deborah number was determined explicitly for a number of fixed bed geometries and, in particular, the specific statistical description of the media necessary to determine these critical conditions was uncovered.

In §4, we modify the theory of Shaqfeh & Koch (1992) to account for the

polydispersity of our dilute polymer sample. We note that the model includes interactions between single polymer chains and single bed particles (with the latter interaction including the mean field screening of the surrounding fixed bed particles). Thus, for a polydisperse polymer sample we simply integrate the previous results over a distribution of molecular weights. In this context, we remain within the dumbbell model for the individual chains and thus the spectrum of molecular weights corresponds to a spectrum of equilibrium lengths and relaxation times. The integration includes quadrature over these spectra. The result of this modification for a log-normal distribution of polymer molecular weight is a broadening in the pore shear rate of the transition originally predicted for a single monodisperse solution of dumbbells. As is expected, this broadening depends on the standard deviation of the molecular weight distribution.

In §4 we also rework the previous theory for the particular bed configuration used in our experiments presented in §3. This particular bed, as described elsewhere (Frattini *et al.* 1991), is disordered but is square symmetric in the plane perpendicular to the mean flow. Such bed structures were not considered in the previous theoretical work (Shaqfeh & Koch 1992) although the physical principles contained in the previous analysis are certainly applicable. Thus, specific calculations for the known bed statistics of our experimental bed are developed and the critical conditions are predicted from first principle calculations.

Finally, in §5 we compare the modified theory with the experimental results. First, we fit an experimentally measured molecular weight distribution with the log-normal distribution to determine the mean and variance of the molecular weight distribution of our sample. We then, using accepted methods to relate the molecular weight distribution to the polymer relaxation time distribution, fit the normalized decay of the birefringence after cessation of flow with the predictions of our modified theory in a good solvent.

Thereafter, a comparison of the steady-state predictions of the polymer stretch and the experimental steady-state birefringence measurements versus the characteristic pore shear rate ($U/\kappa^{1/2}$) is made. Strong qualitative and quantitative agreement is found. Lastly, the transient birefringence measurements (from the initial coiled conformation to the eventual steady-state stretched conformation) are compared, with no adjustable parameters, to the predictions of the time-dependent second moments at various values of the characteristic pore shear rate. While qualitatively the comparison of theory and experiment show agreement, there exist quantitative differences.

2. Experimental

We examine the degree of polymer stretch induced by flow through a dilute fixed bed of randomly positioned fibres using the polarization-modulated flow birefringence method (Frattini & Fuller 1984; Galante 1991; Galante & Frattini 1993). In addition we also simultaneously measure the pressure drop across the bed. The fibre bed construction and its experimental characterization have been described in Frattini *et al.* (1991). In the present work we obtain the exit birefringence of flexible poly(isobutylene) solutions of dilute and semi-dilute concentrations over a range of flow rates corresponding to pore-size Deborah numbers, $U\lambda/\kappa^{1/2}$, ranging from 3 to 25. The following subsection summarizes the essential features of the fibre bed flow cell and the pressure sensing and rheo-optical instrumentation, and describes the preparation and characterization of the test solutions.

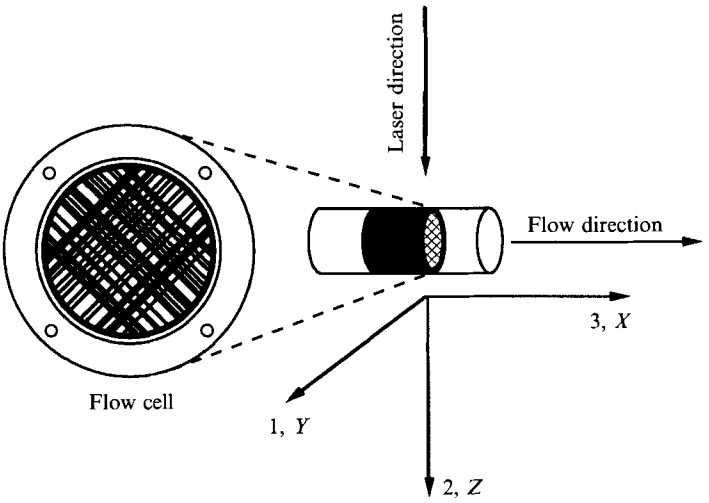

FIGURE 1. The geometry of our fibre bed with the coordinate system used in our analysis. For a photograph of the fibrous bed see Frattini *et al.* (1991).

2.1. *Fibrous bed and flow cell*

The dilute fixed fibre bed used for all experiments is identical to the bed used in Frattini *et al.* (1991), and their work should be consulted for a more detailed description and physical characterization of the bed. The cylindrical housing for the fibre bed, with inner diameter 3.59 cm, mounts an approximately 2.54 cm square block of crossed fibres along its axis. The bed was produced by inserting 492 pieces of hypodermic tubing with outer diameter 0.0203 cm (0.008 in.) through the housing which was later sealed with epoxy. While the fibre positions were random, the orientations were confined to two orthogonal directions in the plane perpendicular to the cylinder axis. This geometry produced two different bed regions (figure 1): the central square porous bed and a second, but different, porous region surrounding this. The resulting central square bed has a volume fraction, ϕ_f, of 0.0247 and a Darcy pore size, $\kappa^{1/2}$, of 0.0486 cm. The bed length, L_{bed}, is 2.54 cm (1.0 in.) or approximately 50 pore lengths. The laser beam was positioned along the diagonal of the central block maximizing exposure of the sampled polymer particles to the crossed fibre media. The insertion of pressure taps at both ends of the bed (the position was 0.2 cm from last fibre) allowed pressure drop measurements to be made concurrently with optical measurements. The pressure taps were connected to a Validyne DP15-TL differential pressure transducer (± 5 p.s.i. and ± 20 p.s.i. membranes, accuracy – $\pm 0.5\%$ FS) and a CD15 sine wave demodulator with high-pressure tubing to determine the pressure difference between these two points during flow.

A dual-reservoir piston drive mechanism is employed to impose steady flow through the bed in the direction of the cylinder axis, as described previously (Frattini *et al.* 1991). In the present work, piston movement was accomplished by a screw assembly (13 rev/in.) driven by a computer-controlled Compumotor CPLX83-150 stepper motor. The motor has a resolution of 5000 steps rev^{-1} and an accuracy of ± 6 arc s^{-1}. The motor could attain a 'step' in velocity within 1/2500 of a revolution. The 2.82 N m of available torque easily handled any loads that we encountered. The flow rate through the bed was calculated from the velocity of the piston, U_{piston}, corrected for the differences in flow resistance within the square bed structure and the surrounding, lower resistance, bed sectors. The bulk flow velocity, U, through this central square bed

was a factor 0.668 less than U_{piston}. Flow velocities of 0.01 to 3.0 cm s^{-1} were easily attainable. The flow cell is mounted horizontally directly onto the optical rail described in §2.2. The observation point at the fibre bed exit was positioned within, at most, two screening lengths of the last fibre in the bed. The active optical path along the diagonal of the central block was 3.12 cm (Frattini *et al.* 1991).

Initiation of an experimental run involved the 'step' of the motor to the desired velocity, producing a bulk plug flow in the crossed fibre bed. Polymers traverse the porous cell, sample the velocity gradient fluctuations within the bed and eventually exit the bed. Optical sampling was obtained at the end of the bed and, since the bed was initially full, this is equivalent to sampling the polymers in a reference frame moving with the bulk velocity, U. In other words, the polymers emerging from the bed at time t have sampled the bed for a length of time t.

2.2. *Optical theory and instrumentation*

A measure of the conformation of a collection of polymers can be described by two averaged quantities: the average amount of stretch, measured by the second moment of the polymer end-to-end vector, and the orientation of that stretch. These two quantities can be directly related to two measurable optical quantities, the birefringence and the extinction angle, respectively, which can simultaneously and independently be obtained using polarization-modulated polarimetry.

The magnitude of the birefringence of a medium is defined as the difference of the principal eigenvalues of the real part of the effective refractive index tensor of the continuum sample. Physically it manifests itself in materials that unequally retard light waves which are linearly polarized in different directions. Microscopically, net polarizability must be produced by some dielectric anisotropy in the material structure. One can imagine a solution consisting of polymers stretched and aligned producing such an anisotropy. Structurally, a linearly polarized light wave will, in general, retard differently when polarized along the length of the polymer chain backbone as opposed to when it is polarized perpendicular to that chain. Thus, the birefringence is related to some measure of the average conformation of the polymers, specifically, the second moment of the distribution of the end-to-end distance vector. The derivation relating the second moments of the polymer end-to-end vector to the index of refraction tensor is well known (Kuhn & Grun 1942; Peterlin 1961) and consists of treating the polymer as a set of connected retarding elements.

The second moment of the end-to-end distance vector, $\boldsymbol{R}$, in a Cartesian system can be related to the index of refraction tensor as follows:

$$\operatorname{dev}(n_{ij}) = A \operatorname{dev}\langle R_i R_j \rangle, \tag{1}$$

$$A = \left[(\alpha_1 - \alpha_2)\frac{2\pi}{45}\frac{(n^2+2)^2}{n}\right] 2\nu\beta^2, \tag{2}$$

$$\beta^2 \equiv \frac{3}{2Nb^2}, \tag{3}$$

where dev denotes the deviatoric part of the tensor, $(\alpha_1 - \alpha_2)$ is the difference of the eigenvalues of the polarizability tensor of each retarding element, n is the isotropic part of the index of refraction tensor, ν is the number of chains per unit volume, N is the number of idealized segments per chain, and b is the length of each segment. The bracketed term in (2) is the traditional stress-optical coefficient multiplied by the Boltzmann energy, kT. Thus, the refractive index tensor is proportional to the second-moments tensor.

Defining the birefringence, $\Delta n'$, as the difference in the principal eigenvalues of the index of refraction tensor we have

$$\Delta n' \sin(2\chi) = 2A\langle R_1 R_3\rangle, \tag{4}$$

$$\Delta n' \cos(2\chi) = A[\langle R_3 R_3\rangle - \langle R_1 R_1\rangle], \tag{5}$$

where χ is the extinction angle and represents the angular difference between the optical and experimental reference frame, and 1 and 3 represent the two principal axes perpendicular to the laser beam defined specifically by the experimental setup (see figure 1). Note that because of the symmetry of our flow cell, the probability density of polymer conformation will always be square symmetric about the mean flow direction for all time. Thus, we configured our optical setup such that the experimental and optical reference frames were collinear as described below. It follows that, for all our experiments, χ was zero and (4) and (5) reduce to

$$\Delta n' = A[\langle R_3 R_3\rangle - \langle R_1 R_1\rangle]. \tag{6}$$

Therefore, the measurement of the birefringence is a direct probe of the difference of the second moments, $\langle R_3 R_3\rangle - \langle R_1 R_1\rangle$.

A polarization-modulated polarimeter (Galante 1991) was used to measure the linear birefringence of the polymer flows. The polarimeter consisted of an Eifle Inc. mounting system and photodiode detector, a Uniphase Helium-Neon laser (632.8 nm), Karl Lambrecht polarizing optics and lenses, and a Hinds International photo-elastic modulator. The laser beam was initially focused with a 500 mm lens placed ahead of the first polarizer. The beam then passed through a polarizer oriented azimuthally at 90° to an arbitrary laboratory axis, a photoelastic modulator at 45°, the flow cell, and finally a second polarizer at −45°. The alignment procedure is found in Galante (1991). The intensity of the emerging laser beam was measured and processed by two EG&G PARC 5208 heterodyning lock-in amplifiers. These amplifiers decomposed the signal into its first and second harmonics with respect to the frequency of the photoelastic modulator, I_ω and $I_{2\omega}$. These two signals along with the zero-frequency reference, I_{dc}, were sent to a Nicolet digital oscilloscope for storage and final transfer to a computer for data analysis. These three observables are related to the birefringence, $\Delta n'$, and extinction angle, χ, as follows:

$$I_\omega / I_{dc} = 2J_1(A_c)\sin(\delta)\cos(2\chi), \tag{7}$$

$$I_{2\omega}/I_{dc} = 2J_2(A_c)[1-\cos(\delta)]\sin(2\chi)\cos(2\chi), \tag{8}$$

where J_n is the nth Bessel function of the first kind, A_c is the value of the amplitude of the photoelastic modulator at which $J_0(A_c) = 0$, and δ is the retardance of the sample. Values of the Bessel function were found experimentally and varied slightly from theoretical values (maximum deviation 3%) owing to phase lags, small non-idealities in the photoelastic modulator amplitude setting, and small unavoidable deviations from theoretical alignment in the laboratory. The retardance, δ, is related to the birefringence as follows:

$$\delta = -2\pi \Delta n' L/\lambda_L, \tag{9}$$

where λ_L is the wavelength of the laser and L is the active optical pathlength. As stated before, the azimuthal optical axis was aligned such that it was collinear with the experimental flow axis. This was accomplished through a simple rotation of the elements of the optical train in unison until the $I_{2\omega}$ observable did not deviate from its baseline value during flow, thus complying with the assumption $\chi = 0$. In all

experiments the two ratios, given in (7) and (8), were measured and the resulting extinction angle and birefringence were calculated.

2.3. *Polymer solutions*

The polymer solutions investigated in this paper are a combination of high-molecular-weight polyisobutylene (PIB), low-molecular-weight polybutene (PB), and trichloroethylene. This fluid is very similar to the M1 fluid, a Boger fluid, examined in Sridhar (1990). However, unlike M1, a range of solution concentrations in the dilute and semi-dilute regime were examined.

The solid high-molecular-weight PIB ($4–6 \times 10^6$ g mol^{-1}, Aldrich no. 18,149-8) was solvated in the trichloroethylene in a ratio of approximately 1:100 for about one week. This produced a working concentrate from which more dilute solutions could be made. This concentrate was prepared such that the smallest amount of solvent was present to fully solvate the PIB. The low-molecular-weight PB (MW 950, Parapol, Exxon no. 81330) was then added to this concentrate as a bulk viscosifier. Polybutene ($\mu = 355$P @ 18.9 °C; $\rho = 0.85$ g cm^{-3}), is known to behave as a Newtonian liquid at all but extreme deformation rates (in shear) because of its low molecular weight. We shall investigate the elasticity of the polybutene in the flow history of the stochastic fibre bed via birefringence measurements discussed in §3.

This three-component solution was then placed in a vacuum chamber to evaporate a large percentage of the trichloroethylene, which in turn increased the characteristic relaxation time of the polymers in solution. This increased relaxation time allowed flow velocities to be relatively low while maintaining a large Deborah number. In addition, a longer relaxation time meant greater resolution in all the experimental measurements. The solution was mixed daily and kept under vacuum for approximately one month followed by ambient mixing for one week to remove any concentration gradients produced by the evaporation.

While the polydispersity of the PIB was reported to be $4–6 \times 10^6$ g mol^{-1} by the manufacturers, our own gel permeation chromatography experiments suggest a broader distribution of molecular weights. Using a Waters chromatograph, consisting of a Waters 510 pump, U6K injector, 3 Shodex columns and a Waters 410 differential refractometer, we found a large percentage of the polymers lie in the $2–20 \times 10^6$ g mol^{-1} range. We shall use the molecular weight distribution found in these experiments in our analysis in §5.

Solutions at PIB concentrations (by weight) of 50, 100, 333 and 1000 p.p.m. were produced. The critical concentration at which the domains of the coiled polymers at equilibrium overlap, C^*, can be calculated to be around 1000 p.p.m. (Quinzani *et al.* 1990). It is expected that the dilute regime will lie at or below this concentration. The shear viscosity, η, for the 333 p.p.m. solution was measured at 294 K and was found to have a constant value of 225 P over a range of shear rates from 0.1 to 50 s^{-1}. All viscosity measurements of the PIB Boger fluids were performed on a Rheometrics Dynamic Analyzer RDA II. A cone-and-plate geometry was used with a gap of 25 μm and an angle of 0.02 rad.

3. Results

Polyisobutylene solutions of different PIB concentration (50, 100, 333 and 1000 p.p.m.) were subject to the sudden inception of a constant flow rate through the porous fibre bed. Measurements of the birefringence and the extinction angle were taken in order to directly and non-invasively probe the polymer's conformation. In

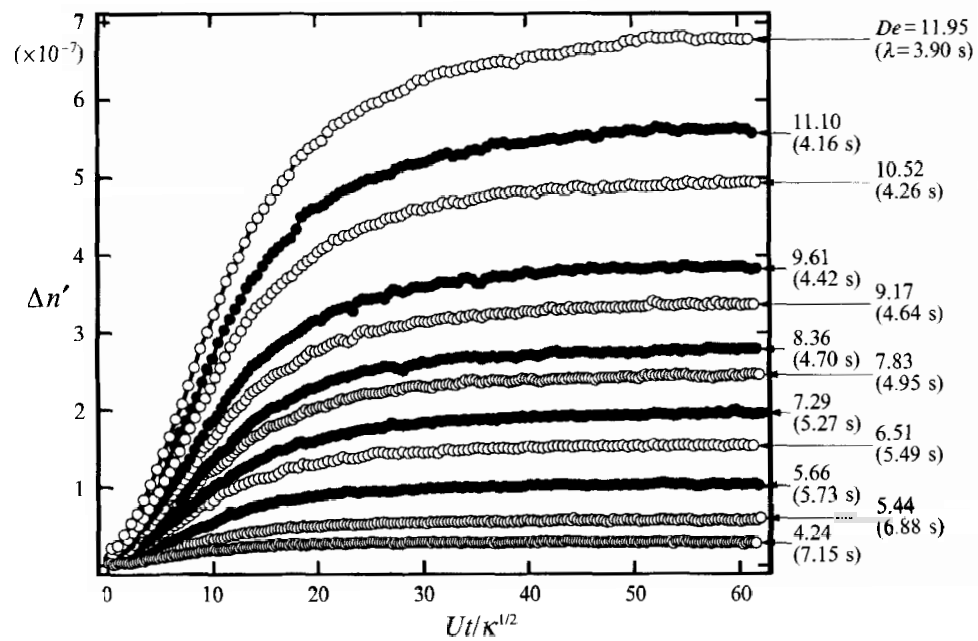

FIGURE 2. Transient birefringence for a 333 p.p.m. PIB solution at various values of the pore-size Deborah number, shown on the figure together with the respective relaxation times for each flow. Each set of data points represents an average over 3 or 4 separate runs. Systematic error is on the order of the size of the plot symbols.

addition, measurements of the pressure drop across the fibre bed were concurrently made. Each polymer solution was subjected, by varying the mean flow velocity, to a number of flows over a wide range of pore-size Deborah numbers. The pistons maintained a constant velocity for approximately 60 pore lengths (recall that the bed length is 50 pore lengths), at which time the flow was stopped. The birefringence measurement was continued thereafter, until the polymer's relaxation produced a decay of the signal voltage to its equilibrium baseline value. All data were then converted into values of the birefringence and the extinction angle, χ. We confirmed that the latter remained zero throughout the experiment. The decay of the birefringence signal, due to the polymers' relaxation from their bed-induced stretched conformation, provided a measure of the characteristic relaxation time for the polymer. As a measure of this relaxation time, we fit the decaying signal with an exponential, thus inferring a time constant for the decay. A discussion and fit to a spectrum of relaxation times is given in §5. Because of the possibility of polymer degradation, a 'leap-frog' run sequence was employed; namely, after every increase in the velocity a previous or reference velocity was rerun to document any permanent decrease in the birefringence signal at a given pore-size Deborah number. For the discussion *in this section*, the relaxation time used in determining the pore-size Deborah number *will be based on the timescale obtained through the exponential fit of the experimental relaxation data for each flow*, $\bar{\lambda}$.

3.1. *Birefringence data*

Figure 2 shows a typical example of *transient* birefringence data for the polyisobutylene solutions during flow. The birefringence for a 333 p.p.m. solution is plotted against a laboratory time which has been made dimensionless. Physically the dimensionless time represents the number of pore lengths an average polymer emerging from the bed has

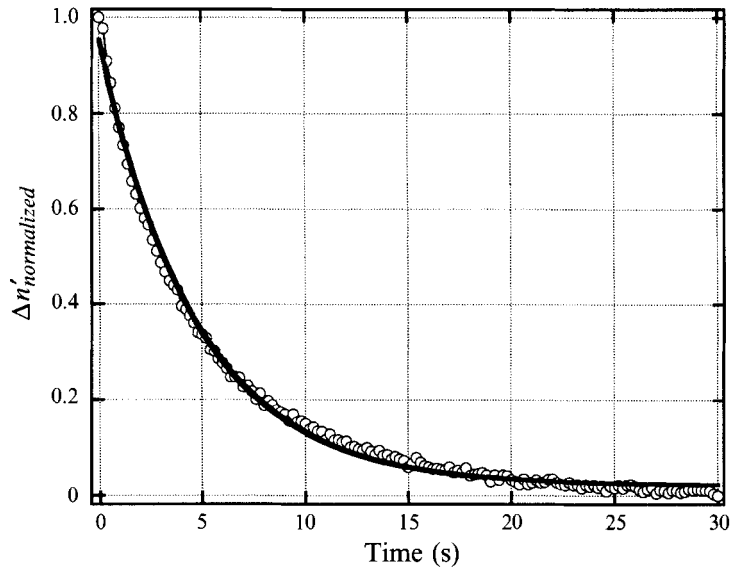

FIGURE 3. Relaxation of the birefringence for a 333 p.p.m. PIB solution after being subjected to flow through a fibre bed at $U/\kappa^{1/2} = 4.05$, corresponding to a pore-size Deborah number of 14.01 (symbols). The heavy line is an exponential fit of the form $\Delta n' = A + B\mathrm{e}^{-t/\lambda}$ where the empirical value of $\bar{\lambda}$ was 3.46 s.

traversed. The data are shown for a number of different flow velocities and their corresponding pore-size Deborah numbers are also presented. Each data set is an average of 3 or 4 separate runs.

At $t = 0$ a step change to the desired flow velocity was created. The polymers traverse the bed and hydrodynamically interact with the fixed bed particles, causing them to stretch in the direction of flow on average. The graph shows a monotonic increase in the amount of birefringence, corresponding to increased stretch, as a function of the pore lengths traversed and reaches a steady state value which increases with Deborah number. In §3.2 concurrent measurements of the pressure drop across the bed are shown which further confirm that the polymers are being stretched as opposed to simply becoming aligned segmentally. This increase in the birefringence along with measurements of the extinction angle indicate the polymers are, on average, being stretched and this stretch is in the direction of the bulk flow. Thus, we see a direct confirmation that the polymers are stretched in a dilute fixed bed.

The number of pore lengths required to reach a steady state is approximately the same *for intermediate values of the Deborah number* ($De \leqslant 9$): approximately 30. In other words, it is the number of polymer interactions with fibre bed particles which determines the time necessary to produce a steady-state conformation distribution. As the Deborah number is increased, however, the number of pore lengths required to reach steady state also increases.

As mentioned previously, at the end of each transient run the flow was stopped and the birefringence signal decayed to its baseline value as the polymers entropically recoiled. Figure 3 shows the relaxation data for the same 333 p.p.m. solution of PIB (once again the average of 3 runs) after cessation of flow ($De = 14.01$), along with a floating baseline-exponential fit as a function of laboratory time. This plot is representative of the relaxation data for all other solutions and Deborah numbers. The data sequence begins with the first data point collected after the flow ceases. The

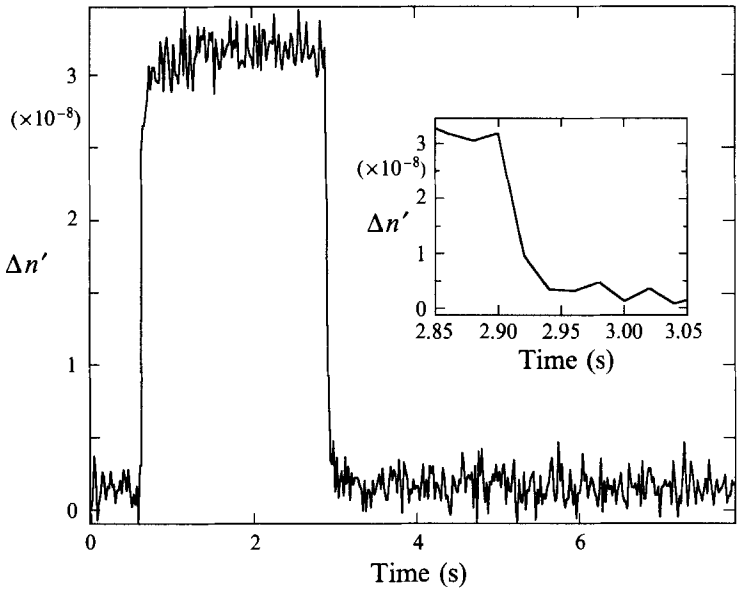

FIGURE 4. Transient birefringence data for the flow of the pure polybutene solvent through the fibre bed at a characteristic pore shear rate, $U/\kappa^{1/2}$. Flow initiation is at 0.5 s and flow cessation is at 2.9 s. The inset shows an expanded view of the decay of the birefringence due to entropic recoil.

maximum value of birefringence ($\Delta n' = 1.02 \times 10^{-6}$) has been normalized so that its value is unity. The exponential fit accompanying the plot is of the form

$$\Delta n'_{norm} = A + B\exp(-t/\bar{\lambda}), \tag{10}$$

where A and B are simply fitting parameters while $\bar{\lambda}$ is some average characteristic relaxation time of the polymer. All relaxation times were found in this way and then used to calculate the experimental Deborah number reported for each run. The relaxation times obtained using this method closely matched those obtained through an exponential fit of the decay of the first normal stress difference after cessation of shear as measured by a Rheometrics RDA-II rheometer using a cone-and-plate geometry. Both techniques produced relaxation times for the 333 p.p.m. solution at 21 °C of approximately 3 s. As expected, the extinction angle measured during this entropic recoiling remained at zero.

Since the bulk viscosifier, polybutene, is also a polymer, it can, in principle, also produce a birefringence signal. Even though the polymer has a low molecular weight and will undergo much less deformation relative to the high molecular weight PIB, it does comprise the bulk of the fluid. Figure 4 shows a transient run of a solution comprising only the bulk viscosifier, polybutene. The birefringence is plotted against laboratory time. The graph shows inception of flow at $t = 0.5$ s and cessation of flow (expanded in the figure inset) at $t = 2.9$ s. While the increase in birefringence is measurable, its magnitude is small (2 %) when compared with the 1000 p.p.m. solution which exhibited birefringence values above 1×10^{-6}. However, for very dilute PIB solutions (i.e. 50 and 100 p.p.m. solutions), this additional signal cannot be neglected. A common method of removing this effect is outlined by Phillippoff (1964). This method involves *vectorially* subtracting the effect of the polybutene. In principle, this can be accomplished by obtaining a separate transient record of the polybutene's birefringence. Fortunately this task was made considerably easier owing to the characteristics of the flow cell and polybutene. First, the porous cell produces an

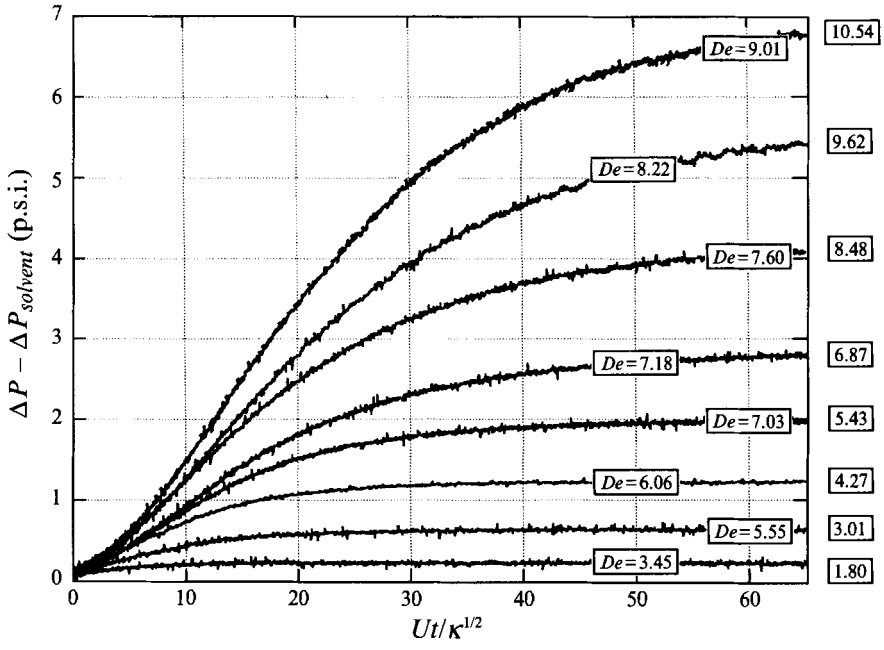

FIGURE 5. Transient pressure drop data for the flow of a 1000 p.p.m. PIB solution, above the PB solvent baseline, at various values of the pore-size Deborah number. The numbers on the right show the value of the steady-state data normalized by the pressure drop of the PB solvent alone.

average alignment of the stretched polymers in the direction of flow regardless of polymer size. Therefore, any vectorial subtraction reduces to scalar subtraction. In addition, as figure 4 shows, the relaxation time of the polybutene sample is two orders of magnitude smaller than that of the PIB. Because the birefringence of the polybutene sample attains a steady-state value and also decays to its baseline value on a timescale (0.02 s) which is much smaller than that of the PIB, it is unnecessary to run two different polymer solutions. In other words, the PB polymers in solution attain their steady-state conformation 'instantaneously' relative to the time necessary for the PIB to attain their steady-state conformation. Therefore, the PB contribution to the birefringence signal can be removed by subtracting the baseline birefringence value (produced solely by the presence of PB) found immediately after inception of flow. *This technique is employed in all our experiments and thus all references to the birefringence of the PIB ssolutions will be to the birefringence produced solely by the PIB in solution.*

3.2. *Pressure drop data*

Pressure drop measurements across the bed were made simultaneously with measurements of the birefringence. If only segmental alignment of the polymer backbone were occurring without any significant polymer stretch, the resistance to flow would not increase. Therefore, measurement of the pressure drop across the bed offers a check on our interpretation of the birefringence measurements as implying stretch of the entire polymer coil.

In figure 5 we show the transient pressure drop for a number of flow velocities as a function of the dimensionless flow time for the 1000 p.p.m. solution. The pressure drop shown is the solvent pressure drop subtracted from the total pressure drop. In other words the pressure drop plotted represents the additional pressure drop due to the presence of the PIB polymer. As with the birefringence, the inception of flow causes an

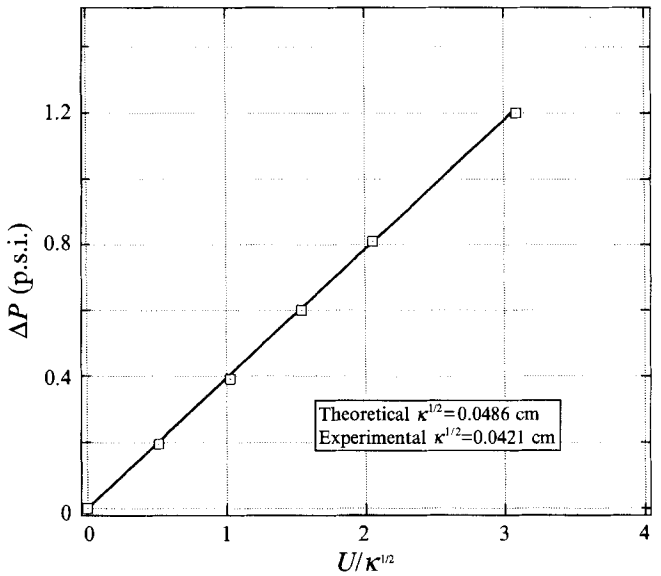

FIGURE 6. The steady-state values of the pressure drop across the fibre bed for the pure polybutene solvent as a function of the pore shear rate (symbols). The line shows a linear fit to the experimental data.

increase in the pressure drop across the bed. This increase eventually reaches a steady-state value which increases with the pore-size Deborah number. To the right of the figure is shown the factor by which the pressure drop is greater than the Newtonian solvent value. For the higher flow rates the additional 1000 p.p.m. of PIB produced a ten-fold increase in the pressure drop over the solvent pressure drop, showing a large increase in the flow resistance. This unambiguously demonstrates that large polymer stretch and not just segmental polymer alignment occurs in the bed.

To determine the pressure drop associated with the solvent and also to check the linear relationship between the pressure drop and the flow rate for a Newtonian fluid, additional runs were taken with polybutene. In figure 6, the steady-state pressure drop for just the Newtonian polybutene solvent is shown along with a linear fit. As expected the data points produce a linear plot intersecting the origin. From the linear fit an experimental calculation of the Darcy pore size, $(UL_{bed}\mu/\Delta P)^{1/2}$, can be made using Darcy's Law. The experimentally determined pore size was 0.0421 cm which represents a -13.37% deviation from the theoretically determined value, $\kappa^{1/2}$, of 0.0486 cm.

The striking similarity between the transient nature of the additional pressure drop (figure 5) and the birefringence shown previously (figure 2) suggests a direct relationship between the two observables. To demonstrate this relationship we plot in figure 7 both the transient birefringence and polymer contribution to the pressure drop for a single flow velocity ($De_{pore} = 7.18$). Two different ordinates, for the two observables, are used and scaled to produce a close visual comparison. This graph shows a direct correlation between the increase in the pressure drop across the bed due to the presence of the polymer and the increase in the amount of polymer stretch. This convincingly demonstrates that the increase in flow resistance within the bed is due to the elongation of the polymer molecules.

To further investigate this relationship, measurements of the steady-state birefringence are plotted against the steady-state value of the additional pressure drop due to the presence of the polymer (figure 8), with both measurements taken

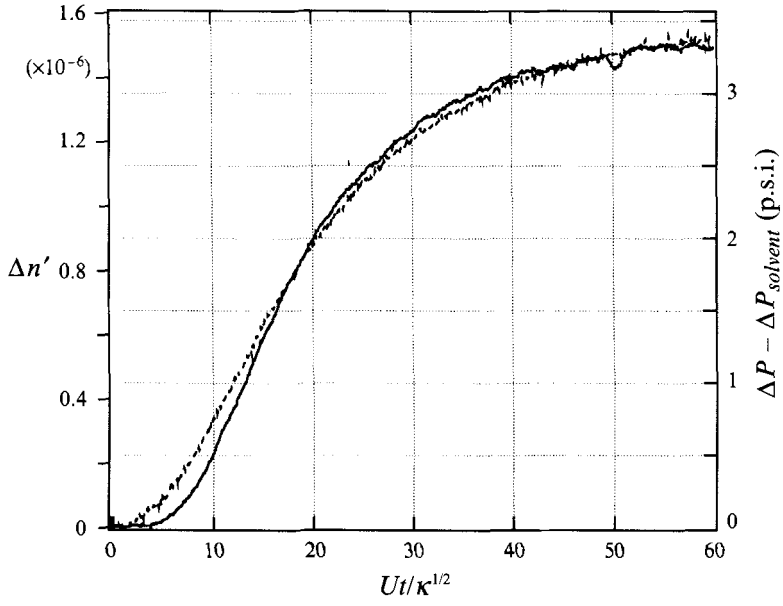

FIGURE 7. Transient birefringence, $\Delta n'$ (left ordinate, ——), and addition of pressure drop due to the PIB (right ordinate, – – –), of the 1000 p.p.m. solution for a single flow rate ($De_{pore} = 7.18$). The two ordinates are scaled visually for comparison. The birefringence data are shifted 2 pore lengths to account for the distance between the end of the bed and the analysing windows.

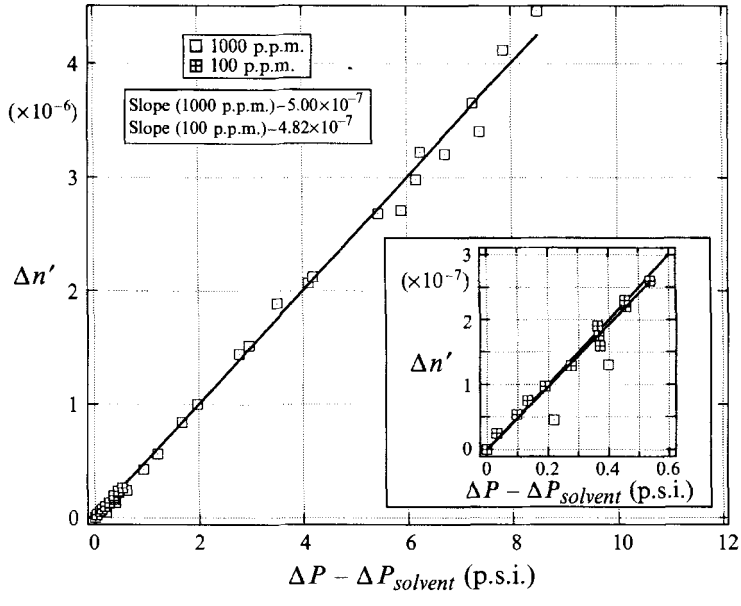

FIGURE 8. Steady-state $\Delta n'$ plotted against steady-state ΔP of the 100 and 1000 p.p.m. solutions for a number of flow velocities. Linear fits to the data for the two solutions accompany the plot. The inset graph is simply an enlargement of the region where the 100 p.p.m. data resides.

simultaneously, at a number of flow velocities for both the 1000 and 100 p.p.m. solutions. The remarkable linear relationship between the two quantities demonstrates that a simple proportionality constant relates the birefringence to the additional pressure drop and this proportionality constant is independent of the flow rate for the

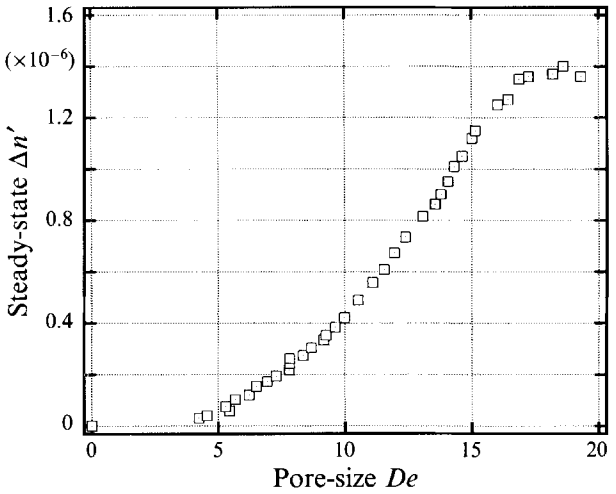

FIGURE 9. Steady-state birefringence values for the 333 p.p.m. PIB solution plotted against the pore-size Deborah number. Systematic error is on the order of the size of the plot symbols.

range of flow rates shown. Thus, the pressure drop across the bed builds as the chain elongates or, in essence, the flow energy is transferred to elastic deformation in the chain.

A linear regression of the data for both concentrations was calculated and the two linear plots have been added to the graph. The proportionality constant between the two observables is then simply the slope of the linear fit. Equally noteworthy is the fact that the proportionality constant for the two solutions differs only by 4% even though the solutions differ in polymer concentration by an order of magnitude and reside, as will be shown, in different concentration regimes. This then strengthens the assertion made above that the increased friction factor, due to the presence of polymers, is a result of significant chain elongation and not simply a local segmental alignment of the polymer backbone.

3.3. *Experimental analysis*

Figure 9 shows the steady-state values of birefringence from figure 2 plotted against the respective experimental pore-size Deborah number for each run. The graph exhibits a characteristic 'sigmoidal' shape seen at all other concentrations. Relatively little increase in the birefringence was noted for Deborah numbers less than 5. At values greater than 5 a strong increase in the steady-state birefringence is observed. The birefringence continues to increase until a Deborah number of around 17 is reached. At this point a permanent decrease in the value of the birefringence obtained at the reference velocity is encountered. The values of the steady-state birefringence cease to increase significantly at higher values of the Deborah number, as shown, in what appears to be the onset of polymer degradation due to polymer scission.

This degradation is documented more clearly in figure 10. In this graph an initial sweep of velocities was made with a 'fresh' PIB solution of 1000 p.p.m. The solution was subjected to progressively larger velocities (larger pore-size *De*) until we suspected significant polymer degradation had occurred. The solution was then stored, untouched, for 2 days. A second velocity sweep was then conducted on the same solution at the same ambient temperature. Assuming no polymer degradation had occurred, we would expect the solution to reproduce the same steady-state birefringence values since the relaxation times would be identical at the same temperature. However,

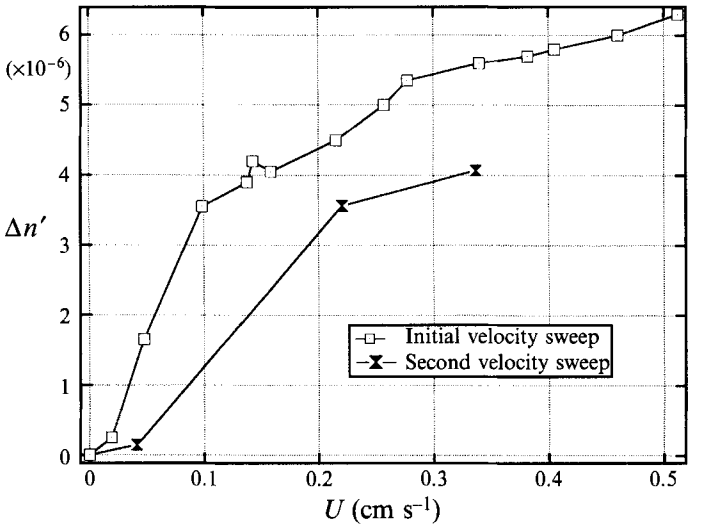

FIGURE 10. Evidence of polymer degradation for the 1000 p.p.m. PIB solution. Steady birefringence values measured during an initial, increasing sweep of velocities is shown, in addition to those for a second velocity sweep after polymer degradation was suspected.

the second velocity sweep showed a dramatic and permanent decrease in the steady-state birefringence values at any given flow rate, which we argue is a result of polymer scission.

Returning to figure 9, our data suggest that a critical Deborah number demarking a quantitative change in the chain elongation, De_{crit}, exists at a value of approximately 5. Since this value is $O(1)$, we are supported in our view that the pore size is the appropriate lengthscale (and thus $U/\kappa^{1/2}$ is the appropriate shear rate) in calculating the De. Since the pore size is apparently the important hydrodynamic lengthscale, it is the velocity gradient fluctuations at this scale and not at the scale of the individual bed fibres that produce the stretch observed in the experiments. This also appears correct when comparing De with the fibre Deborah number, De_{fibre}, defined as

$$De_{fibre} = U\bar{\lambda}/a, \tag{11}$$

where a is the fibre radius. For our bed De_{fibre} is approximately five times larger than De. Using the fibre radius as a lengthscale, therefore, would produce a De_{crit} of around 25. However, one would expect theoretically that the effects of any such fibre-related phenomena would occur at a De_{fibre} of order one (Harlen *et al.* 1992; McKinley *et al.* 1993).

Since the constant relating the birefringence to the second moments of the end-to-end vector of the polymer is unknown, the increase in birefringence, in and of itself, does not necessarily mean 'large' polymer stretch is occurring within the bed. Even if this constant were known, one cannot rule out the possibility that segmental alignment, which would produce a birefringent sample, could be occurring without any significant polymer stretch. However, there are three pieces of evidence to suggest large polymer stretch is indeed occurring. First, as mentioned previously, evidence of polymer degradation was found. Presumably only large deformations of a given polymer would induce chain scission. Second, measurements of the additional steady-state pressure drop due to the presence of the PIB polymer were shown in §3.2 to be an order of magnitude larger than the pressure drop associated with the solvent alone. Only large polymer deformation could produce such a phenomenon.

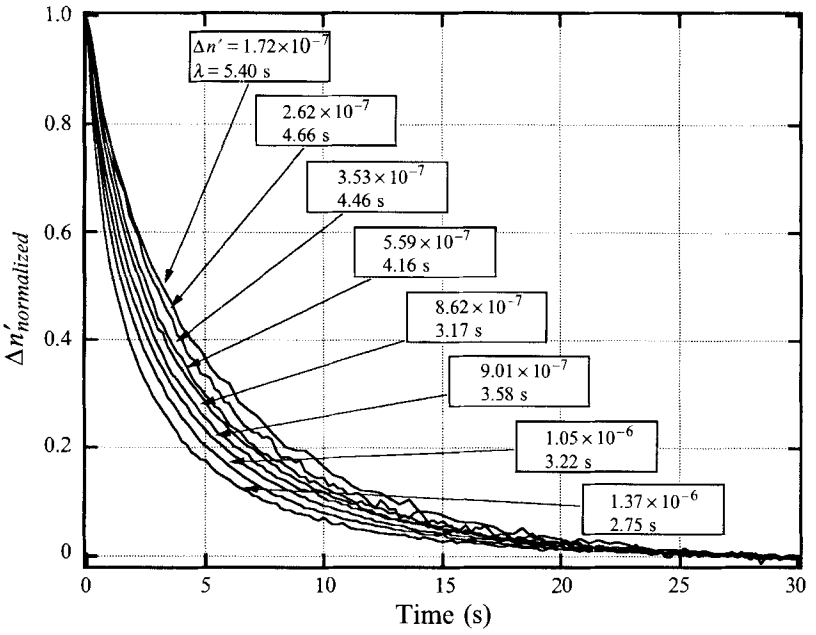

FIGURE 11. A plot of the normalized relaxation decays of the birefringence for the 333 p.p.m. PIB solution after flow through the fibre bed produced a steady value of the birefringence. Shown are decays after steady flow at various pore-size Deborah numbers, hence various initial steady values of the birefringence. Also included are corresponding relaxation times, $\bar{\lambda}$, found through an exponential fit.

Lastly, we can compare our results to those of Geffroy & Leal (1990). In their work they measured the birefringence of M1, a similar fluid, subjected to an extensional flow via a two-roll mill. Steady extensional flow is a strong flow, known to produce large deformation of polymers (Bird *et al.* 1978). M1 comprises polyisobutylene (same manufacturer and distribution), polybutene, and kerosene, instead of trichloroethylene, as the solvating agent. In addition, the concentration of PIB in M1 is 2440 p.p.m. which is in the non-dilute concentration regime. The birefringence measurements obtained by the extensional and porous bed flows can be compared, to a first approximation, by normalizing the birefringence with concentration and comparing the two flows at any given post-critical Deborah number where the birefringence has increased significantly. For an extensional flow Deborah number of 7, which one knows produces a large polymer stretch, a birefringence value, normalized by concentration, of 3.6×10^{-9} p.p.m.$^{-1}$ is found, while a birefringence value of 1.2×10^{-9} p.p.m.$^{-1}$ is found in the porous bed at comparable values of the pore-size Deborah number. While these values are different, they are of the same order of magnitude, suggesting that a dilute fixed fibre bed produces polymer deformation comparable to that in the two-roll extensional flow. Note that since the first effect in our porous bed of increased PIB concentration is to increase the specific birefringence obtained at a given value of *De*, the birefringence values produced in the two flow experiments may indeed be much closer quantitatively than suggested above.

Another phenomenon observed throughout our experiments is displayed in figure 11. In this graph the normalized birefringence relaxation curves for a number of runs taken at *different* Deborah numbers (and thus different steady-state values of the birefringence) are plotted against real laboratory time. In addition, values for the empirical relaxation time, $\bar{\lambda}$, and steady-state birefringence are shown. We note that as

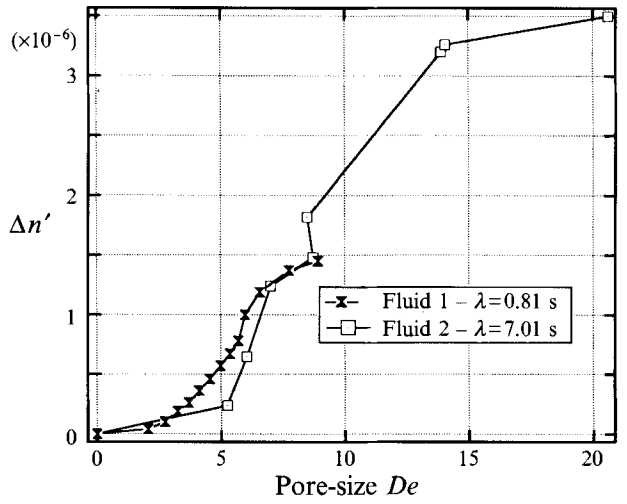

FIGURE 12. A plot showing the ability of the pore-size Deborah number to correlate the steady-state birefringence data of two 1000 p.p.m. PIB solutions with average relaxation times, $\bar{\lambda}$, of 0.81 s and 7.01 s.

the Deborah number increased and the polymers were subsequently stretched to a greater degree, the corresponding characteristic relaxation time decreased. We are uncertain as to the true cause of this effect. However, two possible mechanisms seem likely. First, the conformation-dependent relaxation times could be a manifestation of the spectrum of relaxation times existing on each chain as predicted, for example, by the Rouse many-linked chain (Bird *et al.* 1978). Thus, our results could be explained by the relaxation modes of the smaller time constants becoming 'excited' as the pore-size Deborah number is increased. As this occurs the total relaxation signal would comprise to a larger extent these smaller relaxation modes, and hence the *average* relaxation time represented by one empirical $\bar{\lambda}$ would decrease.

Another possibility, however, follows from our gel permeation chromatography experiments which show that the majority of this polymer sample lies between the range of $2\text{–}20 \times 10^6$ g mol^{-1}. Through known scaling laws (refer to §4.2), a spectrum of molecular weights implies a spectrum of relaxation times. Therefore, a different spectrum of relaxation modes are 'excited' in a polydisperse sample at different pore-size Deborah numbers. However, unlike higher frequency modes in the single chain, this mechanism entails 'exciting' or stretching polymers of *smaller* molecular length with increasing flow rate. *In our judgement solution polydispersity is the primary cause of conformation-dependent values of* $\bar{\lambda}$, *and we will assume that each chain in the solution can be characterized by a single relaxation time, depending on its molecular weight.* In §5 we will return to this phenomenon and discuss the relative merits of this assumption.

In a separate set of experiments, we investigated the ability of the pore-size Deborah number to correlate our steady-state data. Two solutions of equal PIB concentration, but differing polymer relaxation times, were prepared by increasing the ratio of low-viscosity solvent (trichloroethylene) to high-viscosity solvent (polybutene). Precautions were taken to ensure that the final concentrations of PIB in both solutions were identical. Figure 12 shows the steady-state data for two solutions with different relaxation times (0.81 and 7.01 s) plotted against the pore-size Deborah number. Because of the upper bound on flow velocities in our experimental system, the range of pore-size Deborah numbers accessible to experiments using the low-relaxation-time

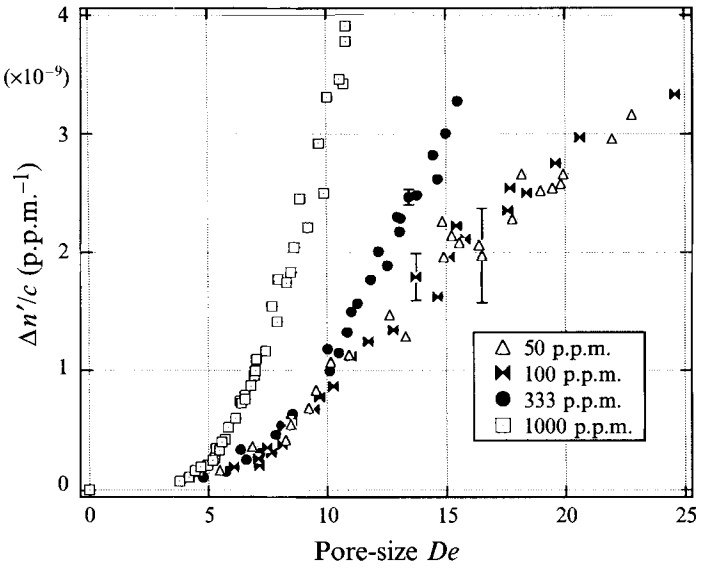

FIGURE 13. Specific steady-state birefringence for 50, 100, 333 and 1000 p.p.m. PIB solutions plotted against the pore-size Deborah number. The error bars increase with decreasing PIB concentration because the birefringence is normalized with concentration.

solution did not include the full spectrum of Deborah numbers for the high-relaxation-time solution. Even though the relaxation times differ by an order of magnitude, the two data sets tend to superpose, showing the ability of the pore-size Deborah number to correlate the steady-state birefringence data.

Finally, we compare the steady-state data obtained by experiments on four PIB solutions (50, 100, 333 and 1000 p.p.m.) to examine the effects of concentration in our data. In all four solutions the trichloroethylene/polybutene composition was kept a constant. Although the estimation of the value of the equilibrium overlap threshold C^* (de Gennes 1979) was 1000 p.p.m., an experimental evaluation of the actual concentration at which the polymer solution enters the non-dilute regime during flow can be determined from our data. Figure 13 shows a compilation of data for the four concentrations. The steady-state values of the birefringence divided by the concentration of the solutions are plotted against the pore-size Deborah number. In a truly dilute concentration regime there will be no interaction between different polymer molecules, and therefore any addition of polymers will increase the birefringence linearly. By normalizing the four sets of data with concentration, we expect to see data in the dilute regime superpose. This occurs for the 50 and 100 p.p.m. solutions. The specific birefringence for the 333 p.p.m. solutions begins to deviate from the specific birefringence for the 50 and 100 p.p.m. concentrations at a Deborah number of around 10. Beyond $De = 10$, the normalized birefringence for the 333 p.p.m. solution increases at a rate greater than that for the 50 and 100 p.p.m. solutions. In other words, above a Deborah number of 10 the 333 p.p.m. solution produces a larger stretch per polymer than the lower-concentration solutions. For concentrations between 100 and 333 p.p.m. the polymers in solution begin to interact with each other at some point in our flow experiments. Like the 333 p.p.m. solution, the specific birefringence for the 1000 p.p.m. solution also deviates from the specific birefringence for the 50 and 100 p.p.m. solutions. However, this deviation occurs at a smaller Deborah number of around 5. Once again, for $De \geqslant 5$ the birefringence increases at a rate greater than that of the lower-concentration solutions. Therefore, the prediction of C^* using the

equilibrium scaling arguments ($\sim$ 1000 p.p.m.) differs from our experimentally measured transition concentration by almost an order of magnitude, demonstrating directly that dynamic polymer–polymer interactions can be significant in a solution which is dilute at rest. This is interesting since it confirms that the polymer's stretching increases the lengthscale of polymer–polymer interactions relative to that in the equilibrium state. Note that the hydrodynamic interaction length should scale with the polymer's largest dimension which increases as the polymer undergoes stretch.

Even though it is shown that the transition from dilute to non-dilute concentrations occurs dynamically between 100 and 333 p.p.m. it is interesting to note that when this distinction is made the transition depends on the magnitude of polymer stretch. If figure 13 includes only data up to a Deborah number of 10, it would appear that the transition concentration would lie between 333 and 1000 p.p.m. Thus, these data strongly suggest that the transition from the dilute regime to non-dilute regime during flow is conformation dependent.

4. Hydrodynamic theory

We now seek to interpret our experimental results in the light of the existing theoretical description of polymer stretch and conformation change in dilute fixed beds as described by Shaqfeh & Koch (1992). This section includes a complete mathematical characterization of the fixed fibre bed used in the experiments. The polymer sample used in our experiments is fairly polydisperse, while the theory of Shaqfeh & Koch (1992) includes consideration of dumbbell models with only a single relaxation time. In order to extend this theory for comparison with our experiments using polydisperse polymer samples, we average the theoretical results over a distribution of molecular weights which corresponds (near equilibrium) to a commonly recognized distribution of relaxation times.

4.1. *Bed theory*

In a detailed analysis, Shaqfeh & Koch (1992) demonstrated that for *dilute* beds the largest contribution to the averaged equation describing the evolution of polymer molecules (modelled as dumbbells) comes from the long-range hydrodynamic interactions. In this context, 'largest' refers to the leading-order term in an expansion for small bed solids volume fractions. Also 'long-range' refers to scales comparable to the Darcy pore size in the bed, which, because of the assumed diluteness, is much larger than the characteristic dimension of the bed particles (i.e. the radius of the fibres for a fibre bed). On the scale of the bed pore, the fibres can be treated as lines of screened force. In addition, if one also assumes that the polymer solution is sufficiently dilute, then one can restrict a kinetic theory describing the evolution of the polymers to include only single interactions between a polymer and a bed fibre. Multi-fibre interactions can then be included as additions to this basic theory via cluster expansion techniques which have been developed in the context of many other transport problems (Hinch 1977). This theoretical approach to stochastic flow problems is supported by its successful prediction of measured values of tracer particle orientation in fixed bed flow (Frattini *et al.* 1991).

We first review the theory as applied to flows of dumbbells through fixed beds. In general, the dimensionless equation relating the rate of change of the end-to-end vector, $\dot{\boldsymbol{r}}$, and the local velocity gradient in the bed, $\nabla_x \boldsymbol{u}$, becomes

$$\dot{\boldsymbol{r}} = \boldsymbol{r}\cdot\nabla_x \boldsymbol{u} - h(\boldsymbol{r})\frac{\boldsymbol{r}}{2De}. \tag{12}$$

In (12) all spatial lengths x have been made dimensionless with $\kappa^{1/2}$, The Darcy pore size in the bed, all velocities with U, the mean flow velocity in the bed, time with $U/\kappa^{1/2}$ and the end-to-end vector, r, with R_g, the equilibrium radius of gyration; h is any function governing the restoring force of the dumbbell. In this work both Hookean and FENE dumbbells will be considered. In the former case $h = 1$ and in the latter $h = R^2_{max}/(R^2_{max} - r^2)$ where R_{max} represents the maximum point of extension relative to R_g, where

$$R_g^2 = 12D/\xi. \tag{13}$$

In (13) D is the diffusivity of the Dumbbell and ξ is the relaxation frequency associated with the spring. Note that R_g is the equilibrium radius of gyration *for a Hookean spring* (which is close to the value for a FENE dumbbell). The averaged equation describing the probability density of configuration, $\langle \Omega(r) \rangle$, for homogeneous, dilute, random beds is (cf. Shaqfeh & Koch 1992)

$$\frac{\partial \langle \Omega \rangle}{\partial \tau} - \tfrac{1}{2}\nabla_r \cdot (r\langle \Omega \rangle) - \nabla_r \cdot \boldsymbol{d}^h \cdot \nabla_r \langle \Omega \rangle = 0, \tag{14}$$

where $\tau = t/\lambda$, ∇_r is the gradient with respect to the polymer's end-to-end vector, and $\boldsymbol{d}^h$ is the conformational diffusion tensor which includes diffusion created by the hydrodynamic interactions of the polymer with the bed particles. It takes the form (in indicial notation)

$$d^h_{ij} = \tfrac{1}{2}[\tfrac{1}{3}\delta_{ij} + B_{ikjn} r_k r_n]. \tag{15}$$

The tensor B_{ikjn} is a certain velocity-gradient correlation function that contains information concerning the manner in which the polymers change conformation during an interaction with a bed fibre as well as how this change is correlated with previous polymer–fibre interactions. The calculation of this tensor is the key piece of statistical information necessary to describe the conformation change of the dumbbell model.

Since, in general, a simple solution for $\langle \Omega(r) \rangle$ is difficult, it is more convenient to develop equations for the moment-of-inertia tensor (second-moment tensor) $\overline{rr}$, defined

$$\overline{rr} = \int rr \langle \Omega \rangle \, \mathrm{d}r. \tag{16}$$

From (15) we have (see Shaqfeh & Koch 1992)

$$\frac{\mathrm{d}\overline{r_j r_k}}{\mathrm{d}\tau} + h\overline{r_j r_k} - \tfrac{1}{3}\delta_{jk} - B_{jmkn}\overline{r_m r_n} = 0. \tag{17}$$

In deriving (17) the pre-averaging approximation has been used in the case of the FENE dumbbell. Thus, as a first approximation $h(r^2/R^2_{max})$ is replaced with the averaged quantity $h(\bar{r}^2/R^2_{max})$. Pre-averaging is only a reliable approximation when the distribution function, Ω, is strongly peaked (Tanner 1985). Note that the moment-of-inertia tensor serves as an important measure of polymer conformation change in many flows of dilute and semi-dilute polymer solutions (Bird *et al.* 1978). In addition, the birefringence of a dilute solution can, under the proper conditions, be a direct measure of the average second moment of the polymer coils. In the experiments described in §3 our conditions and solutions have been carefully chosen such that the birefringence is directly proportional to the difference in the principal eigenvalues of $\overline{rr}$.

It is clear from (17) that, within the approximations of the theory described above,

the time-dependent second moment of $\overline{rr}$ can be completely described for a given bed geometry once the tensor B_{jkmn} is calculated. The fibre bed utilized for these experiments is, as described in §2, square-symmetric. The calculation of B_{jkmn} for this new bed structure (outlined in the Appendix) gives

$$B_{jkmn} = \left(\frac{De}{4\pi^2}\right)\left[\frac{\sqrt{11}}{3}\pi^3\left(\frac{\ln(1/\phi)}{\ln^2(\kappa^{1/2}/a)}\right) + \frac{2\sqrt{11}}{3}\pi^2\left(\frac{\ln(1/\phi)}{\ln^2(\kappa^{1/2}/a)}\right)^2(0.30\ldots)\right]\delta_{j3}\delta_{k3}(\delta_{kn}-\delta_{k3}\delta_{n3}) + \left(\frac{De}{4\pi^2}\right)\left[\sqrt{\frac{11}{27}}\frac{\pi^2}{2}\left(\frac{\ln(1/\phi)}{\ln^2(\kappa^{1/2}/a)}\right)^2(0.11\ldots)\right](\delta_{j1}\delta_{k2}\delta_{m1}\delta_{n2}+\delta_{j2}\delta_{k1}\delta_{m2}\delta_{n1}). \quad (18)$$

Defining the two bracketed terms in (18) as β_1 and β_2, respectively, and referring to (17), we find

$$\frac{\mathrm{d}\overline{r_j r_k}}{\mathrm{d}\tau} + h\overline{r_j r_k} - \tfrac{1}{3}\delta_{jk} - \frac{2De\phi\kappa}{\ln(\kappa^{1/2}/a)^2\pi a^2}\beta_1\delta_{j3}\delta_{k3}(\delta_{mn}-\delta_{m3}\delta_{n3})\overline{r_m r_n} - \frac{2De\phi\kappa}{\ln(\kappa^{1/2}/a)^2\pi a^2}\beta_2(\delta_{j1}\delta_{k1}\delta_{m2}\delta_{n2}+\delta_{j2}\delta_{k2}\delta_{m1}\delta_{n1})\overline{r_m r_n} = 0. \quad (19)$$

Finally, defining the three quantities

$$r^2 = \overline{r_i r_i}, \quad r_3^2 = \overline{r_3 r_3}, \quad \rho^2 = \tfrac{1}{2}(\overline{r_1 r_1}+\overline{r_2 r_2}) \quad (20)$$

and noting that

$$r^2 = r_3^2 + 2\rho^2 \quad (21)$$

we obtain

$$\frac{\mathrm{d}r^2}{\mathrm{d}\tau} + h\left(\frac{r^2}{R_{max}^2}\right)r^2 - 1 - \frac{4De\phi\kappa}{\ln(\kappa^{1/2}/a)^2\pi a^2}(\beta_1+\beta_2)\rho^2 = 0, \quad (22)$$

$$\frac{\mathrm{d}r_3^2}{\mathrm{d}\tau} + h\left(\frac{r^2}{R_{max}^2}\right)r_3^2 - \frac{1}{3} - \frac{4De\phi\kappa}{\ln(\kappa^{1/2}/a)^2\pi a^2}\beta_1\rho^2 = 0, \quad (23)$$

$$\frac{\mathrm{d}\rho^2}{\mathrm{d}\tau} + h\left(\frac{r^2}{R_{max}^2}\right)\rho^2 - \frac{1}{3} - \frac{2De\phi\kappa}{\ln(\kappa^{1/2}/a)^2\pi a^2}\beta_2\rho^2 = 0. \quad (24)$$

These equations are equivalent to those determined for polymer conformation in flow through an isotropic fibre bed by Shaqfeh & Koch (1992) even though the functional form of the conformational diffusivity tensor, B_{jkmn}, is different. At this point we will consider only the steady solutions to the moments equations (22)–(24). These solutions can be found easily by setting the time derivatives to zero and solving the resulting set of quadratic equations,

$$r^2 = \frac{-(1-\beta_2\mathscr{D}+\gamma-2\sigma\mathscr{D}\gamma)+[(1-\beta_2\mathscr{D}+\gamma-2\sigma\mathscr{D}\gamma)^2-4\mathscr{D}(\beta_2\gamma+\sigma\gamma^2)(\sigma\mathscr{D}-1)]^{1/2}}{2\mathscr{D}(\beta_2\gamma+\sigma\gamma^2)}, \quad (25)$$

$$\rho^2 = \frac{1}{3}\left(\frac{1-\gamma r^2}{1-\mathscr{D}\beta_2(1-\gamma r^2)}\right), \quad (26)$$

where

$$\mathscr{D} = \frac{2De\phi\kappa}{\ln(\kappa^{1/2}/a)^2\pi a^2}, \quad \gamma = \frac{1}{R_{max}^2}, \quad \sigma = \tfrac{1}{3}(\beta_2-2\beta_1). \quad (27)$$

We see for the Hookean dumbbell ($R_{max} \to \infty ; \gamma \to 0$) that when the rescaled pore-size Deborah number $\mathscr{D} = 1/\beta_2$ there exists no steady solution for the second moment, r^2. Therefore, the critical point for conformation change, as discussed by Shaqfeh & Koch (1992), is governed by β_2 and at $\mathscr{D} = 1/\beta_2$ there exists a sufficient number of stretched polymers such that the second moment of the distribution is unbound. More realistically, the FENE dumbbell, whose stretch is bound by a maximum length (R_{max}), stretches to a large portion of its maximum extensibility at pore-size Deborah numbers greater than the critical value.

4.2. *Modification of theory to include polydispersity*

Because of the effects of the polydispersity of the polyisobutylene used in our experiments (discussed in § 3.3), the theory of Shaqfeh & Koch (1992) must be extended to account for the effects of polydispersity in order to facilitate a meaningful comparison with our data. The technique of averaging over a polydisperse length or molecular weight distribution has been used elsewhere (Fuller & Leal 1980). In this technique it ia assumed that a single relaxation time and single equilibrium radius of gyration are associated with the molecular weight of a polymer and are given by

$$\lambda = \beta_\lambda M^{\nu_\lambda} \tag{28}$$

$$R_g = \beta_g M^{\nu_g}, \tag{29}$$

where λ is the characteristic relaxation time of the polymer (and is not equivalent to the empirically determined $\bar{\lambda}$ in § 3), R_g is the equilibrium radius of gyration, M is the molecular weight of the polymer, and ν_λ and ν_g are the scaling exponents. Since polybutene and trichloroethylene are both good solvents for polyisobutylene a value of $\frac{3}{5}$ is used for ν_g (i.e. the result for self-avoiding random walk (Flory 1953)) and $\frac{9}{5}$ for ν_λ (i.e. the result for a Zimm chain with $\nu_g = \frac{3}{5}$ (Doi & Edwards 1986)).

A log-normal distribution of the molecular weight is assumed for the polymers. This distribution is often employed since it properly characterizes the non-negative value of the weight distribution in addition to the high-molecular-weight 'tail' associated with polydisperse polymer samples (Brandrup & Immergut 1989). The log-normal distribution is given by

$$p = \frac{1}{M\sigma_x(2\pi)^{1/2}} \exp\left\{\frac{-[\log(M) - \mu_x]^2}{2\sigma_x^2}\right\}, \tag{30}$$

where p is probability, and σ_x and μ_x are related to the true standard deviation, σ, and mean, μ, of the log-normal distribution through the relations

$$\sigma = (e^{\sigma_x} - 1)\, e^{2\mu_x + \sigma_x}, \tag{31}$$

$$\mu = e^{\mu_x + 0.5\sigma_x}. \tag{32}$$

Figure 14 shows this distribution with a mean of 1 and various values for the variance, σ.

Equations (28) and (29) then relate the distribution of molecular weights to a distribution of relaxation times and radii of gyration. Thus, each polymer of molecular weight M is treated as if it contains its own single relaxation time and its own characteristic pore-size Deborah number. At any given flow rate, longer polymers are subjected to greater pore-size Deborah numbers than shorter polymers owing to their larger relaxation time. It follows that longer polymers will stretch to a greater degree than shorter polymers at any given flow rate.

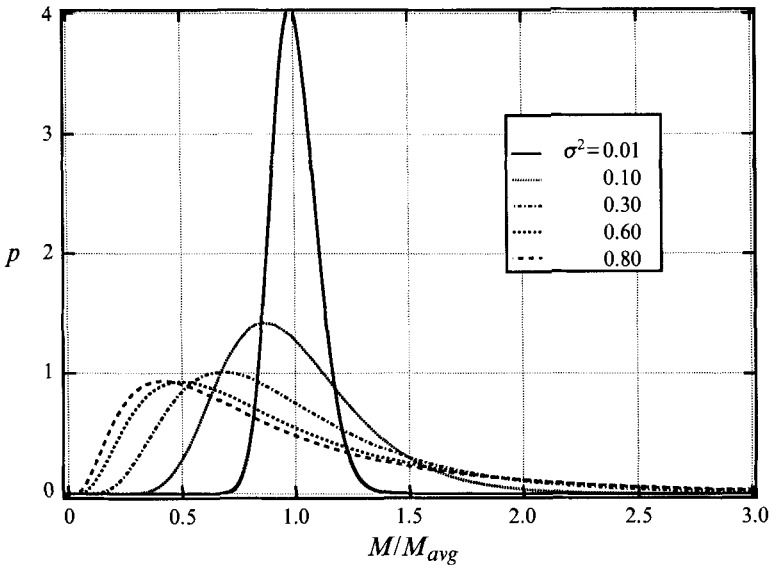

FIGURE 14. Depiction of the log-normal distribution function with a mean, μ, of unity and various values of the variance, σ^2.

To calculate an average birefringence of the polydisperse sample, we further employ the model of Shaqfeh & Koch (1992). For any given molecular weight in the spectrum, a relaxation time and, thus, a Deborah number can be assigned. For each *De* a difference in the second moment can be calculated during the flow (see §4.1). This average can then be scaled with the radius of gyration (Nb^2) for each molecular weight. To calculate an average over the molecular weight distribution of *dimensionless* moments we use the equation

$$\{\langle XX\rangle-\langle YY\rangle\}_p=\int_0^\infty(\langle XX\rangle-\langle YY\rangle)p\,\mathrm{d}M, \tag{33}$$

where $\{\ \}_p$ represents the average over the molecular weight distribution and p is given by (30). This averaged quantity is now related to the solution birefringence by a new constant A' defined as

$$A'=\left[(\alpha_1-\alpha_2)\frac{2\pi}{45}\frac{(n^2+2)^2}{n}\right]3\nu_{total}, \tag{34}$$

where ν_{total} is the total number of polymers per volume in solution and is related to the concentration, c, given here in units of p.p.m. In addition, each value of $\langle XX\rangle-\langle YY\rangle$ has an associated decay with cessation of flow and the average normalized decay of the system can be described by

$$f(t)=\frac{\displaystyle\int_0^\infty \mathrm{e}^{-t/\lambda}[\langle XX\rangle-\langle YY\rangle]_{steady}p\,\mathrm{d}M}{\displaystyle\int_0^\infty[\langle XX\rangle-\langle YY\rangle]_{steady}p\,\mathrm{d}M}. \tag{35}$$

In (35), $f(t)$ represents the time-dependent decay function generated through the integral over exponentials (found from the spectrum of molecular weights) weighted by

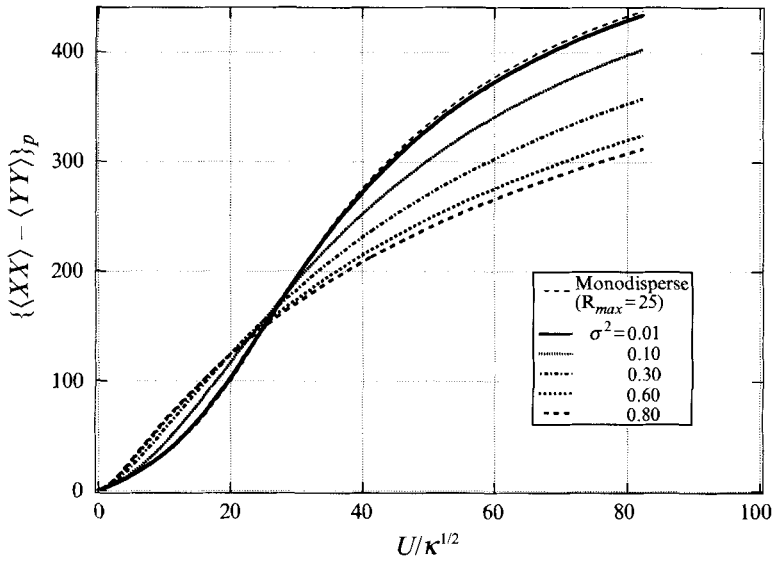

FIGURE 15. Theoretical predictions of $\{\langle XX\rangle - \langle YY\rangle\}_p$, the difference of the second moments, for various values of the variance, σ^2 as a function of the pore shear rate, $U/\kappa^{1/2}$.

the respective magnitude of initial stretch $[\langle XX\rangle - \langle YY\rangle]_{steady}$ and its probability, p. This function will be used in §5 to determine β_λ in (28) through a fit. This method was used to model the conformation-dependent relaxation times found in our experiments (figure 11). Equations (33) and (35) are both defined as integrals over all positive real space. In numerically evaluating these integrals the limits were chosen to coincide with the range of molecular weights determined in our gel permeation chromatograph experiments.

Figure 15 shows the resulting average difference in the second moments plotted against the characteristic shear rate within the bed $(U/\kappa^{1/2})$ for the flow of a polydisperse polymer solution with the molecular weight distribution shown in figure 14. In general, the rate of increase of the moments decreases with increasing polydispersity (the latter increases with increasing σ^2 defined by (31)). Moreover, the apparent 'critical' shear rate (at which the difference in the moments begins to increase significantly), slightly decreases with increasing polydispersity. These effects are primarily due to the presence of a range of molecular weights which undergo a significant diffusive stretch at various pore shear rates. Both effects serve to significantly 'smooth' the transition of the polymer from the polymer's equilibrium coiled conformation to the stretched conformation at high shear rates, suppressing the visibility of a critical pore-size Deborah number.

5. Discussion

Having modified the existing theory of Shaqfeh & Koch (1992) to account for the specifics of bed geometry and polydispersity, a direct comparison of theory to experiment may be addressed. The modified theory at this point still has several unassigned parameters. These include σ^2 – the variation of the polymer molecular weight distribution normalized about the mean, R_{max} – the maximum extensibility of the polymer, β_λ – the coefficient relating the molecular weight spectrum to the relaxation time spectrum, and A' – the coefficient relating the birefringence to the

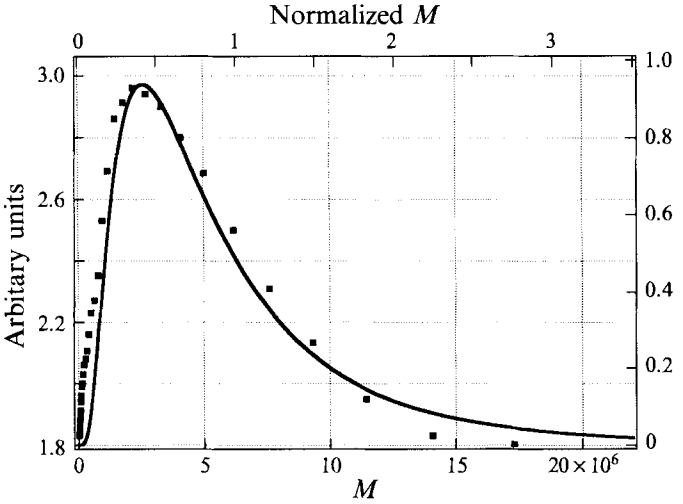

FIGURE 16. The fit of the log-normal distribution ($\sigma^2 = 0.80$) (——) with polydispersity data obtained using a Waters gel permeation chromatography (■).

difference in the second moments. These values must be either determined or approximated in order to quantitatively compare the theory and experiment.

Chromatography experiments were undertaken to determine $\bar{M}_w/\bar{M}_n$ which would define the variance of the molecular weight distribution. In figure 16 a pointwise plot of the polydispersity distribution determined from our experiments is shown. Utilizing this plot a working value of $\sigma^2 = 0.80$ was determined by fitting our log-normal distribution. In addition, the probability of finding a polymer with molecular weight outside the range shown in figure 16 was set to zero and, thereafter, the distribution was renormalized. While this method in no way is an exact characterization of the true distribution, it offers an approximate value from which to proceed.

The estimation of the value of R_{max} offers particular problems not only because of the distribution of the polymers' equilibrium radius of gyration due to the polydispersity of the polymer sample but also because of the stochastic nature of the flow and its resulting effects on the conformation of the polymers. It is unlikely that all polymers at a given molecular weight will, when stretched to a large degree, approach the same maximum length. Rather it is expected that a distribution of highly 'kinked' to highly 'unravelled' polymers will exist. This effect may possibly be amplified by the widely varying flow histories of individual polymers in the bed. Therefore any determination of this parameter should be taken as an order of magnitude approximation.

There are several methods that we can utilize to make this approximation. Peterlin (1961) shows that the maximum birefringence, $\Delta n'_\infty$ for a dilute polymer solution of independently aligned, fully stretched chains, can be given as

$$\frac{\Delta n'_\infty}{nc} = 2\pi\left(\frac{n^2+2}{3n}\right)^2 \frac{N_A N}{M}(\alpha_1-\alpha_2). \tag{36}$$

N_A is Avogadro's number, N is the number of segments in the statistical model, and M is the molecular weight. Using this equation to estimate a value of N, we can determine an approximate *maximum* value for the dimensionless quantity R_{max}. To estimate N we take the value for $(\alpha_1-\alpha_2)$ as 5.96×10^{-24} cm^3 (Chirinos *et al.* 1990) which is determined from values of the stress-optical coefficient, C (Larson 1988), for

the M1 solution in small-strain oscillatory shear flow. As a measure of the order of magnitude of $\Delta n'_\infty$ we utilize the birefringence measurements obtained at the point of polymer degradation from our experiments at 100 p.p.m. concentration. However, we accept the likelihood that the true value of $\Delta n'_\infty$ could be significantly larger than this estimate and, thus, use a value ten times greater to ensure an upperbound estimation for R_{max}. Using these values, we determine the largest possible value of N to be $O(10000)$ (actual value is 7310). Thus, an estimate of the maximum value of R_{max} scaled by the equilibrium radius of gyration would be $7310/7310^{3/5} = 35.12 \sim O(40)$ (using the experimental value of $\Delta n'_\infty$ we find an estimation of the maximum value of $R_{max} = 13.98 \sim O(15)$). Thus, we would expect the true value of R_{max} to lie at or below an $O(40)$ value. The only experimental determination of this parameter was found in the work of Quinzani *et al.* (1990) and McKinley *et al.* (1993). Quinzani *et al.* (1990), who characterized a polyisobutylene solution similar to ours but more concentrated, found a value of R_{max} of 10 for the first and primary mode of a four-mode Bird–DeAguiar model. This value agrees with our estimate made above. In addition, McKinley *et al.* (1993) use a value for R_{max} of 12 for a non-interacting dumbbell model in flow past a single cylinder. Finally, Ng & Leal (1993) found that a value of $N = 1200$ (which would correspond to an R_{max} of 17) well represented their birefringence data on monodisperse polystyrene solutions over a range of flow strength.

For our theoretical predictions a constant value of $R_{max} = 25$ is used. At lower values of R_{max} the rate of stretch, with increasing shear rate, is constantly decreasing. This causes the functional shape of the steady-state moments to be of a slowly 'arching' form rather than the sigmoidal shape encountered in our experiments. A value of 25 retains the sigmoidal shape of our experiments and remains within our $O(40)$ prediction for an upperbound value of R_{max}. Note that in the calculations above we have assumed that there is no molecular weight dependence of R_{max}, though others (Fuller & Leal 1980) have assumed that $R_{max} \sim N$. If we had assumed, for example, that $R_{max} \sim M^{2/5}$ then the variation over the entire molecular weight distribution of our experiments would only be a factor of 2.5. Thus, we shall maintain that R_{max} retains a constant value of 25.

Using the previously mentioned values of $\sigma^2 = 0.80$ and $R_{max} = 25$ we proceed to determine β_λ in (28). This is accomplished through a fit of the relaxation data (obtained through experiments on the 100 p.p.m. PIB solution) to the theoretical predictions (obtained through the integration of exponentials outlined in §4). Figure 17 shows a plot of the decay of the birefringence (normalized to unity) for the 100 p.p.m. solution. The data shown correspond to the decay of the birefringence of the solution after being subjected to a number of flows with pore shear rates, $U/\kappa^{1/2}$, in the range of 4.12–20.16 s^{-1}. In addition, the theoretical results for the functional form of the decay of the difference in the second moments (normalized to unity as defined) for an identical range of bed shear rates is shown for several values of β_λ. We find that $\beta_\lambda = 0.316$ s reproduces the general timescale on which our experimental results decay. In addition, in the secondary graph we can see that the *distribution* of relaxation rates predicted through our theory closely parallels the distribution seen in our experimental results. This distribution is both a function of the polydispersity of the polymer sample (σ^2) and the value of β_λ. The good fit suggests that the values chosen for these two quantities accurately characterizes our polymer system.

It is interesting to note that, by definition, the value of 0.316 s for β_λ represents the relaxation time for the mean molecular weight. This is a significantly lower value than the empirical value of $\bar{\lambda}$ obtained from an exponential fit of $f(t)$ (~ 1.0 s). The reason for this is shown clearly in figure 18. In addition to showing the probability values, p,

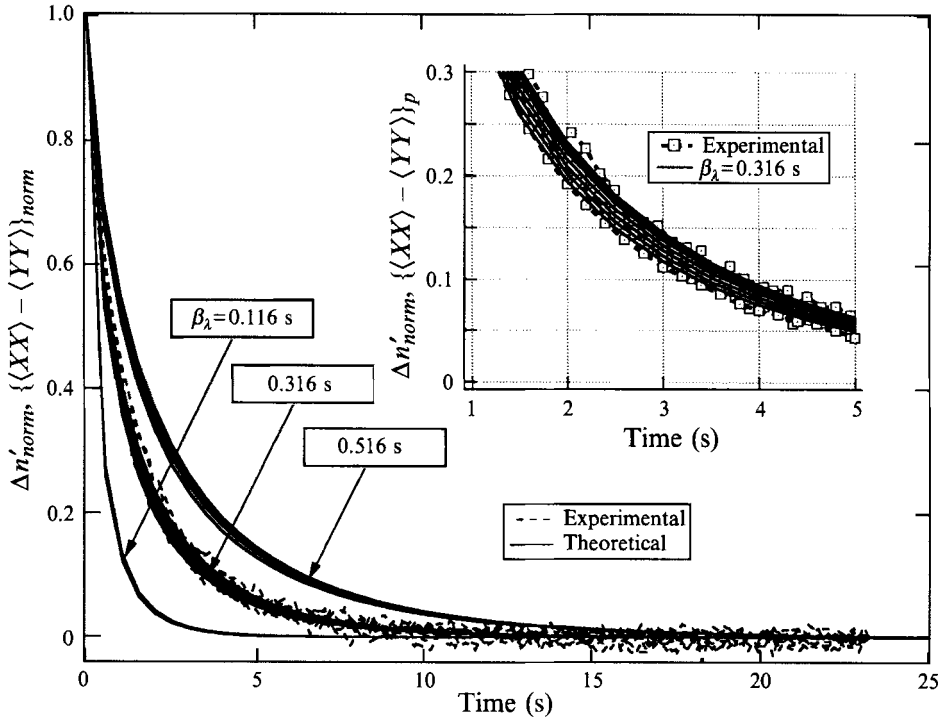

FIGURE 17. Normalized plot of both the decay of the birefringence following cessation of the flow of a 100 p.p.m. PIB solution and the theoretical predictions of the difference in the second moments assuming a polydisperse polymer sample ($\sigma^2 = 0.80$) and values of $\beta_\lambda = 0.116$, 0.316, 0.516 s, where β_λ represents the relaxation time of the mean molecular weight.

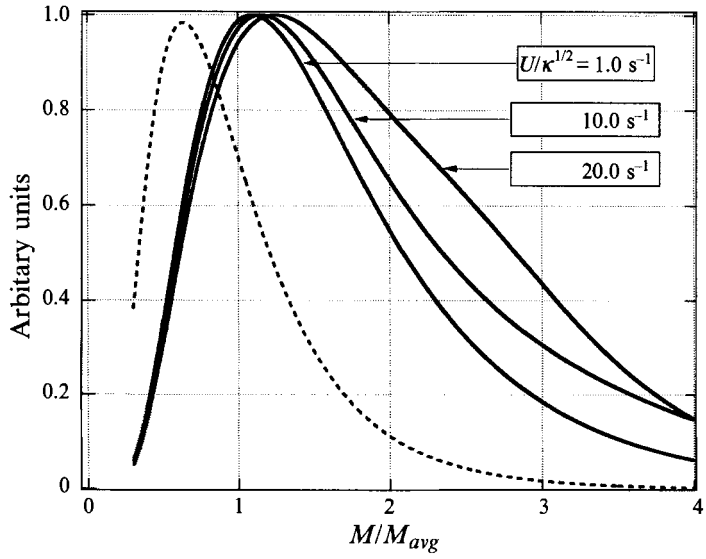

FIGURE 18. Plot of the probability values, p (given by the log-normal distribution function) (– – – –), as a function of the normalized molecular weight in addition to the normalized values of $p\{\langle XX\rangle - \langle YY\rangle\}_p$ (——) which are used to 'weight' individual exponential decays of the second moment in calculating $f(t)$.

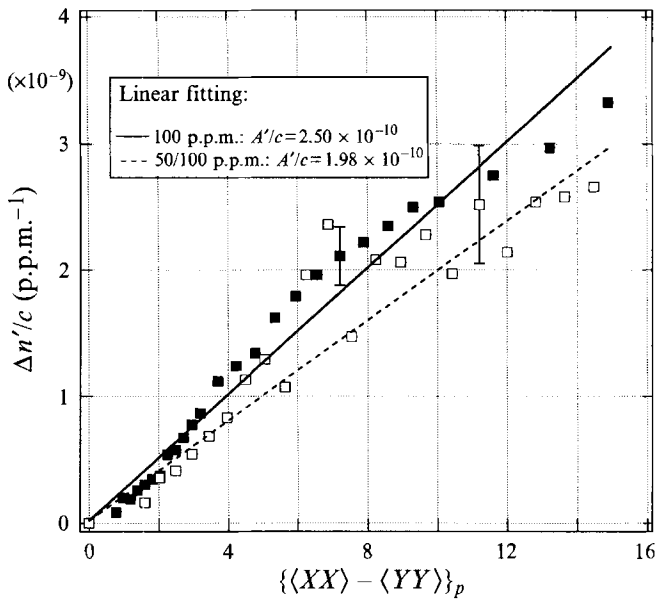

FIGURE 19. Specific steady-state birefringence of the 50 (□) and 100 PIB p.p.m. (■) solutions plotted against $\{\langle XX\rangle - \langle YY\rangle\}_{p,\,steady}$ at the corresponding values of the characteristic pore shear rate $U/\kappa^{1/2}$. Two linear fits are included (one for the 100 p.p.m. data alone and one for the 50 and 100 p.p.m. data collectively) which determine the value of the constant A' relating the index of refraction and second-moment tensor. The errors bars increase with decreasing PIB concentration because the birefringence is normalized with concentration.

as a function of normalized molecular weight, M/M_{avg} (given by the log-normal distribution) we have also plotted the 'weighting' values, $\{\langle XX\rangle - \langle YY\rangle\}_p p$, used to calculate the moments decay, $f(t)$, for pore shear rates of 1.0, 10.0 and 20.0 s^{-1} as a function of normalized molecular weight. We see the time constants that contribute most to the form of $f(t)$ are those with molecular weights approximately two times that of the mode of the molecular weight in the distribution. Thus, even though the relaxation time for the mean molecular weight is 0.316 s, it is the larger-molecular-weight polymers (those with relaxation times of approximately 1 s) which determine the time constant characterizing the relaxation of the second moments.

Finally we determined the value of A' (the coefficient relating the index of refraction and second-moments tensor averaged over the molecular weight distribution) through a linear regression of the steady-state results. Figure 19 shows the steady-state, specific birefringence measurements obtained for the 50 and 100 p.p.m. (dilute) solutions plotted against the difference in second moments, $\{\langle XX\rangle - \langle YY\rangle\}_p$, as predicted by the modified theory. For each specific birefringence datum, the corresponding pore shear rate ($U/\kappa^{1/2}$) is used in the theory to calculate a prediction of the difference in the second moments. Given a theory which perfectly describes the evolution of the average steady-state conformation of polymers, combined with the linear relation between birefringence and the second moments, we would anticipate figure 19 to be a linear plot intersecting the origin with slope equal to the constant, A'/c. We notice that within the experimental error this is essentially what we observe. Small deviations occur between the 50 and 100 p.p.m. solutions that are not apparent in figure 13 (specific birefringence plotted against pore-size Deborah number). This is most likely due to small temperature differences in the 50 and 100 p.p.m. solutions which lead to differing viscosities and,

thus, differing relaxation times. However, within the experimental error the data points for the two solution superpose. Included is the linear fit to both the 100 p.p.m. PIB solution and the collective data of the 50 and 100 p.p.m. PIB solutions. The slope of these fits then determines the value of A'.

Using the slope calculated from the linear fit in figure 19 we obtain the scaling parameter, A', which is then used to provide a comparison of the experiment and theory in figure 20. The specific birefringence for both the 50 and 100 p.p.m. PIB solutions and the difference in the second moments (now scaled with the values of A' determined above) are plotted against the characteristic shear rate in a pore. The characteristic shape, inherent in the theory, matches the observed experimental data. In addition, the point at which the difference in the second moments undergoes a significant increase agrees well with that of the experiment. This point of increase is determined solely by the pre-determined parameters of the theory and, thus, represents a quantitative comparison with experiment.

Finally, a comparison of transient birefringence increase with our theoretical predictions is presented. Figure 21 shows the transient increase in birefringence for the 100 p.p.m. solution from its initially coiled state for a number of flow rates. Once again the flow time is made dimensionless with the mean flow velocity, U, and the pore size, $\kappa^{1/2}$. In addition, the theoretical predictions for the average difference in the second moment at identical values of $U/\kappa^{1/2}$ accompanies the experimental data and are scaled according to the determination of A' found through the linear fit with only the 100 p.p.m. PIB solution data. As with our comparison to the steady-state theoretical predictions, (33) is used. However, in this case the time-dependent equations for the second moments are numerically solved and then the results averaged over the molecular weight distribution at incremental times. As stated previously all bed and polymer parameters are, at this time, specified.

Figure 21 represents our least satisfying comparison between the theoretical and experimental results. While there are deviations in the steady-state or near steady-state values of the moments and birefringence these are, for the most part, within the experimental error. The primary incongruity between the two sets of data stems from a discrepancy in the timescale involved with the polymer stretch. While the number of pore lengths required to reach steady state as predicted by the theory is of the same order as that of the experiments and, in addition, the trend of an increasing number pore lengths necessary to reach a steady state with increasing $U/\kappa^{1/2}$ is reproduced. The range of timescales apparent in the theoretical predictions, however, is not seen in the experimental data. The theoretical transient data at small values of $U/\kappa^{1/2}$ attains a steady state in a shorter distance than the corresponding experimental transient data. Likewise, at large values of $U/\kappa^{1/2}$ the theoretical predictions fall far short of attaining their steady values while the experimental results have essentially reached a plateau. There are a number of factors which could produce this discrepancy. First and foremost is the assumption that our conformation-dependent relaxation times are due solely to the polydispersity of the sample and that there exists a one-to-one correspondence between molecular weight and relaxation time. The presence of a spectrum of relaxation modes per chain could potentially alleviate this problem. Secondly, our log-normal distribution was terminated at low molecular weights by the absence of data in this region. This short-chain cutoff occurred at $M/M_{avg} = 0.3$. The presence of these shorter chains, and correspondingly their shorter relaxation times would contribute to the birefringence at larger values of $U/\kappa^{1/2}$ as these polymers begin to become stretched. Hence, the timescale for growth of the birefringence could potentially decrease. Lastly one must consider the possibility that physical mechanisms

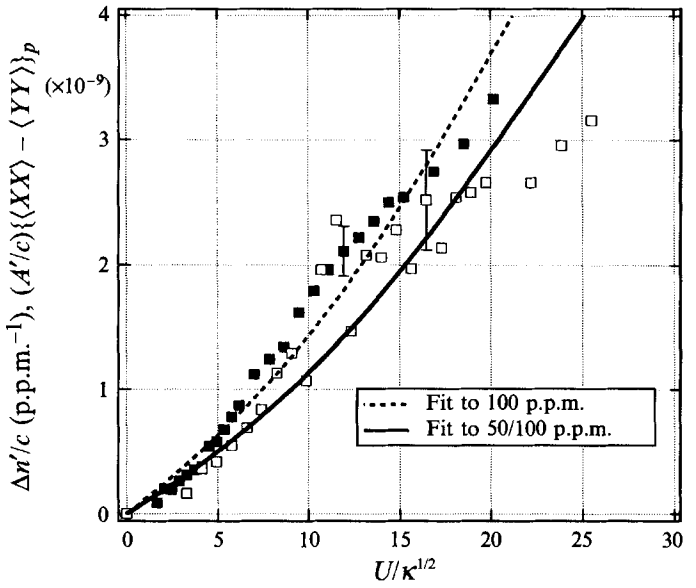

FIGURE 20. Specific steady-state birefringence of the 50 (□) and 100 PIB p.p.m. (■) solutions plotted against the characteristic shear rate. Included are the theoretical predictions of the steady-state averaged difference of the second moments scaled with the values of A' as determined in figure 19.

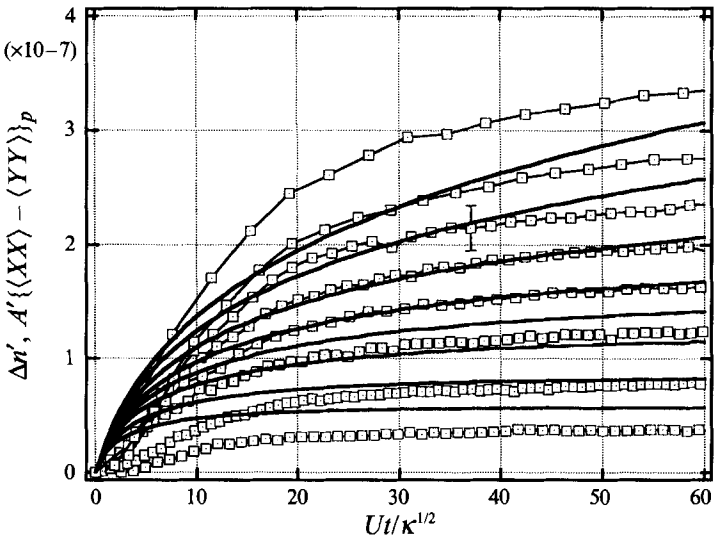

FIGURE 21. Transient results showing the birefringence for the 100 p.p.m. PIB solution (—⊡—) plotted against the dimensionless experimental flow time for characteristic shear rates of 4.12, 5.76, 7.82, 9.47, 11.11, 13.58, 16.87 and 20.16 s^{-1}. Included as the heavy lines are the transient results of the theoretically predicted averaged difference of the second moments for the previously stated pore shear rates. The two ordinates are scaled according to the determination of A' using only the steady-state results of the 100 p.p.m. PIB solution. $\sigma^2 = 0.80$, $\beta_\lambda = 0.316$ s, $R_{max} = 25$.

not included in the theory, specifically the absence of close polymer–fibre hydrodynamics interactions, could play an important role in changing polymer conformation at larger values of $U/\kappa^{1/2}$.

6. Conclusions

To our knowledge, the experimental results we present document the first direct confirmation of large polymer stretch occurring within a dilute disordered fibre bed and provide new insight into establishing porous media flow as a stochastic strong flow. Evidence of polymer degradation and birefringence levels of the same order of magnitude as those produced in two-roller extensional flows establish the ability of the flow to produce significant polymer stretch in the direction of flow even though the fibre bed examined was dilute (2.47%). Furthermore, we have shown that the transient development of the pressure drop across the bed required to maintain a fixed flow rate is directly proportional to the observed birefringence signal, as are the steady-state values. Moreover, this single proportionality constant is independent of polymer concentration and Deborah number. These results represent the first direct microstructural evidence in favour of the hypothesis that large polymer stretch is indeed responsible for the striking increase in hydrodynamic resistance seen for flows of flexible polymer solutions through porous media.

The amount of stretch induced in the polymer chains, obtained through measurements of the linear birefringence, was found to be a function of the distance traversed by the polymer molecules and increased monotonically with increasing pore-size Deborah number. In addition, the results suggest the existence of a critical Deborah number for which flows, characterized by a Deborah number larger than the critical value, produce large changes in a measure of the average polymer conformation. That the value of the Deborah number at this critical point is $O(1)$ ($De \sim 5$), suggested the correct lengthscale characterizing the flow strength or shear rate is apparently the Darcy pore size, which is a measure of the interstitial spaces within the bed and for dilute beds is much larger than the lengthscale of the constituent bed particles. Thus, the primary mechanism for stretch and alignment of the polymeric tracer particles is their interaction with velocity-gradient fluctuations scaling with the characteristic shear rate, $U/\kappa^{1/2}$.

We then demonstrated that the theory by Shaqfeh & Koch (1992) when modified for the specifics of our experiments such as polymer polydispersity and the bed geometry, can predict qualitatively, and in some respects quantitatively, the important features of our experimental birefringence results. This supports the idea that far-field hydrodynamic interactions within dilute porous media can produce a diffusive effect that leads to large polymer stretch. To our knowledge, no other theory of porous media flow to date, employing any of the model geometries proposed in the literature for such media, can produce a comparably accurate description of the chain stretch we observe here in a flexible polymer system.

Finally, it is worth noting that on physical grounds the increased driving pressure required to maintain a constant flow rate through the fibrous bed as the polymer chains elongate is a direct consequence of the elasticity of those chains; namely, a portion of the increased energy input to drive the flow is stored as elastic energy in the deformed macromolecules. As such it is suggested that the stochastic strong flow represented by flow through a dilute random fibrous bed might serve as an alternative means of rheologically characterizing polymer behaviour in highly elongational deformation histories.

More specifically, the diffusive nature of the deformation history of a chain passing through the bed affords it the opportunity to obtain very high degrees of stretch relative to more commonly accepted extensional rheometers, such as the flow history obtained in opposing jets. Indeed, some researchers have suggested that high degrees of polymer stretch may not in fact occur in these other extensional flow geometries and that birefringence measurements made therein saturate at segmental configurations substantially less anisotropic than a highly elongated chain (Cathey & Fuller 1990; Menasveta & Hoagland 1991).

While it is not immediately evident how the so-called extensional viscosity (which might more aptly be termed an elastic material function since it actually measures a normal stress anisotropy) could be extracted from measurements of hydrodynamic resistance in the stochastic strong flow on which we report here, it does seem clear that such pressure drop data obtained on highly elongated flexible macromolecules should at least qualitatively complement the extensional viscosity reported from other experiments wherein the level of chain strain achievable is likely to be substantially less.

Lastly, we speculate that the stochastic strong flow might show promise as a means of rheologically characterizing semi-flexible systems, though rotary Brownian effects (Frattini *et al.* 1991) may become important simultaneously with achievement of critical chain stretch, and we further suggest that some consideration in future be given to the use of the dilute random fibrous bed as a process vehicle to produce critical chain alignment and elongation in situations where such microstructural features are desirable for practical reasons.

The authors would like to acknowledge the support of several organizations for funding this work. First, our research was initiated with support from the Center for Materials Research at Stanford University under the NSF-MRL Program. We would like to thank the National Science Foundation for additional funding through the Presidential Young Investigator Award, grant No. CTS-9057284. In addition we would like to thank the David & Lucille Packard Foundation for a fellowship to E.S.G.S. and the ACS-PRF for their funding through grant 23214-G7. Portions of this work were begun at Carnegie Mellon University during P.L.F.'s tenure on the faculty there and were funded by his Dreyfus Foundation Teacher–Scholar Award and his NSF PYI award (CTS-8552496).

Appendix

As described elsewhere (Shaqfeh & Koch 1992), there are a number of ways to calculate B_{jkmn}. However, the most general method which has been developed heretofore is to relate the flow within the fixed bed to an equivalent stochastic Gaussian field (Shaqfeh & Koch 1992). The tensor B_{jkmn} can then be related to the covariance of this field. If $\boldsymbol{w}(\boldsymbol{x})$ is the stochastic velocity at a point $\boldsymbol{x}$ in this field, then the covariance is defined

$$\boldsymbol{\Delta} \equiv \langle \boldsymbol{w}(\boldsymbol{x})\, \boldsymbol{w}(\boldsymbol{x}') \rangle, \tag{A 1}$$

where the angle brackets now refer to an average over the Gaussian statistics of the field. Since the bed is assumed to be homogeneous, the translational invariance of the system requires that $\boldsymbol{\Delta}$ take the form

$$\hat{\Delta}_{ij}(\boldsymbol{k}, \boldsymbol{k}') = (2\pi)^3 \delta(\boldsymbol{k}+\boldsymbol{k}') f_{ij}(\boldsymbol{k}), \tag{A 2}$$

where the 'hat' refers to the Fourier transform (in both $\boldsymbol{x}$ and $\boldsymbol{x}'$) and where the tensor $f_{ij}(\boldsymbol{k})$ takes the value

$$f_{ij}(\boldsymbol{k}) = (1/V) \langle \hat{\boldsymbol{w}}(\boldsymbol{k})\, \hat{\boldsymbol{w}}'(-\boldsymbol{k}) \rangle, \tag{A 3}$$

with V the volume of the system (in the limit as $V \to \infty$). The tensor B_{jkmn} was derived by Shaqfeh & Koch (1992), in terms of the function f_{jm} as

$$B_{jkmn} \equiv \frac{De}{4\pi^2} \int \mathrm{d}\xi \xi_k f_{jm}(\xi) \xi_n, \tag{A 4}$$

where the integral is over the wavevector $\boldsymbol{\xi}$ lying in the plane perpendicular to the mean flow $\boldsymbol{U}$, i.e. $\xi_j \equiv (\delta_{jm} - \tilde{U}_j \tilde{U}_m) k_m$ and $\tilde{\boldsymbol{U}} \equiv \boldsymbol{U}/|\boldsymbol{U}|$. This theory can be applied to any homogeneous fibre bed upon specification of the orientation distribution function. In previous work the fourth-tensor, B_{jkmn}, was found for isotropic beds of spheres and fibres (Shaqfeh & Koch 1992).

We begin with a working approximation for the dimensionless covariance of the equivalent Gaussian field for a fibre bed:

$$\begin{aligned} \Delta = & \left(\frac{\phi}{\pi a^2}\right) \int_e \mathrm{d}e\, g(e) \int_Z \mathrm{d}Z\, \delta(\boldsymbol{Z}\cdot\boldsymbol{e}) \langle \boldsymbol{u}' \rangle_1 (\boldsymbol{Z} - \boldsymbol{\rho}) \langle \boldsymbol{u}' \rangle_1 (-\rho) \\ & + \left(\frac{\phi}{\pi a^2}\right)^2 \int_e \mathrm{d}e\, g(e) \int_Z \mathrm{d}Z\, \delta(\boldsymbol{Z}\cdot\boldsymbol{e}) \int_{e'} \mathrm{d}e'\, g(e' \mid \boldsymbol{Z}, \boldsymbol{e}) \\ & \times \int_\zeta \mathrm{d}\zeta \langle \boldsymbol{u}' \rangle_2 (\boldsymbol{Z} - \boldsymbol{\rho}, \boldsymbol{e} \mid \zeta, \boldsymbol{e}') \langle \boldsymbol{u}' \rangle_2 (-\boldsymbol{\rho}, \boldsymbol{e} \mid \zeta, \boldsymbol{e}'), \end{aligned} \tag{A 5}$$

where $\langle \boldsymbol{u}' \rangle_1$ is the conditionally averaged velocity disturbance for a single isolated fibre in a porous bed positioned at $\boldsymbol{Z}$ and is a function of $\boldsymbol{\rho}$, the distance in the plane perpendicular to the fibre's orientation, $\boldsymbol{e}$. $\langle \boldsymbol{u}' \rangle_2$ is the correction to the disturbance velocity field created by a single fibre given the presence of a second fibre located a distance ζ away. All calculations will be completed to leading order in bed volume fraction. The covariance is made dimensionless with U^2. In addition, ϕ is the solids volume fraction and a is the radius of the fibre. Finally, $g(\boldsymbol{e})$ is the orientation distribution function and describes the probability of finding a fibre with orientation $\boldsymbol{e}$, and $g(\boldsymbol{e}' \mid \boldsymbol{Z}, \boldsymbol{e})$ is the probability of finding a second fibre of orientation $\boldsymbol{e}'$, given a fibre at position $\boldsymbol{Z}$ with orientation $\boldsymbol{e}$. In the square-symmetric bed used in our experiments and assuming no orientational correlations we have

$$g(\boldsymbol{e}) = \tfrac{1}{2}\delta(e_1 - 1) + \tfrac{1}{2}\delta(e_2 - 1), \tag{A 6}$$

$$g(\boldsymbol{e}' \mid \boldsymbol{Z}, \boldsymbol{e}) = \tfrac{1}{2}\delta(e_1' - 1) + \tfrac{1}{2}\delta(e_2' - 1). \tag{A 7}$$

Note that the approximation given by (A 5) takes into account interparticle interactions through two-particle interactions, which are the leading-order effects for small solids volume fraction. Higher-order interactions could be included and would create terms which are higher order in powers of $1/\ln(1/\phi)$ or equivalently $1/\ln(\kappa^{1/2}/a)$, (cf. (A 17) and (19)).

Taking the Fourier transform of (A 5) produces a relation between the transform of the covariance and the transform of the disturbance velocity, namely

$$\begin{aligned} \hat{\Delta}_{ij} = (2\pi)^3 \delta(\boldsymbol{k} + \boldsymbol{k}') \Bigg[& 2\pi \left(\frac{\phi}{\pi a^2}\right) \int \mathrm{d}e\, g(e)\, \delta(\boldsymbol{k}\cdot\boldsymbol{e}) \langle \hat{\boldsymbol{u}}' \rangle_1 \langle \hat{\boldsymbol{u}}' \rangle_1 \\ & + \frac{2\pi}{2} \left(\frac{\phi}{\pi a^2}\right)^2 \int \mathrm{d}e\, g(e) \int \mathrm{d}\zeta \langle \boldsymbol{u}' \rangle_2 \langle \hat{\boldsymbol{u}}' \rangle_2 \Bigg], \end{aligned} \tag{A 8}$$

where $\langle \hat{\boldsymbol{u}}' \rangle_1$ and $\langle \hat{\boldsymbol{u}}' \rangle_2$ represent the transforms of $\langle \boldsymbol{u}' \rangle_1$ and $\langle \boldsymbol{u}' \rangle_2$, respectively. From

(A 2), we see that the bracketed term is equivalent to f_{ij}. In order to determine the transform of the far-field disturbance velocity created by a single isolated fibre in a porous bed, a solution of the appropriate Brinkman's equations including a line forcing must be determined. The line force solution for Brinkman's equations in a fibre bed is given as the solution of

$$\mu\nabla^2\langle u_i'\rangle_1 - \frac{\partial\langle p\rangle_1}{\partial x_i} - \mu K_{ij}^{-1}\langle u_j\rangle_1 = f_i\,\delta(\boldsymbol{x}), \tag{A 9}$$

$$\frac{\partial\langle u_i\rangle_1}{\partial x_i} = 0, \tag{A 10}$$

$$K_{ij}^{-1} = \left(\frac{8\phi}{a^2\ln(1/\phi)}\right)\delta_{i3}\,\delta_{j3} + \left(\frac{6\phi}{a^2\ln(1/\phi)}\right)(\delta_{ij} - \delta_{i3}\,\delta_{j3}), \tag{A 11}$$

where the right-hand side of equation (A 9) is the Dirac delta function forcing term, μ is the viscosity, and K_{ij} is the permeability tensor for our square-symmetric bed (Jackson & James 1986). In addition, 3 represents the direction of the mean flow and f_j is the force per length on the fibre which, for a fibre of orientation $\boldsymbol{e}$ is given by

$$f_j = \frac{4\pi\mu}{\ln(\kappa^{1/2}/a)}(\delta_{jk} - e_j e_k)\,u_k^l + \frac{2\pi\mu}{\ln(\kappa^{1/2}/a)}e_j e_k\,u_k^l, \tag{A 12}$$

where u_j^l is the fluid velocity at the fibre. We solve Brinkman's equations for the conditionally averaged disturbance velocity with a single fibre held fixed by first Fourier transforming (A 9) and then letting u_j^l be the bulk flow, $U_j = U\delta_{j3}$. Thus, we find

$$\langle\hat{u}_i'\rangle_1 = \frac{4\pi U}{\ln(\kappa^{1/2}/a)(\xi^2 + 4b - \tilde{\xi}_3^2 a)}(\delta_{i3} - \xi_i\,\xi_3), \tag{A 13}$$

where $\boldsymbol{\xi}$ is the wavevector in the plane perpendicular to $\boldsymbol{e}$ and b is given by

$$b = \frac{2\phi}{a^2\log(1/\phi)}. \tag{A 14}$$

To find the correction to the conditionally averaged disturbance velocity which includes the first effects of fibre–fibre interactions, we let u_j^l be given by the configurationally averaged velocity disturbance created by the presence of a second fibre located a distance ζ away. Thus, we obtain

$$\langle\hat{u}_i'\rangle_2 = \frac{1}{\mu(\xi^2 + 3b)}(\delta_{ij} - \tilde{\xi}_i\,\tilde{\xi}_j)f_j$$

$$+ \frac{-b}{\mu(\xi^2 + 4b - \tilde{\xi}_3^2 b)(\xi^2 + 3b)}(\delta_{i3}\,\delta_{j3} - \tilde{\xi}_3(\delta_{i3}\,\tilde{\xi}_j + \tilde{\xi}_i\,\delta_{j3}) + \tilde{\xi}_3^2\,\tilde{\xi}_i\,\tilde{\xi}_j)f_j, \tag{A 15}$$

where f_j in (A 15) is given by

$$f_j = \frac{4\pi\mu}{\ln(\kappa^{1/2}/a)}(\delta_{jk} - e_j e_k)\langle u_i'\rangle_1(\zeta) + \frac{2\pi\mu}{\ln(\kappa^{1/2}/a)}e_j e_k\langle u_i'\rangle_1(\zeta). \tag{A 16}$$

Combining all our terms in (A 4), (A 8), (A 13) and (A 15) and completing the integrals we have

$$B_{jkmn} = \left(\frac{De}{4\pi^2}\right)\left[\frac{\sqrt{11}}{3}\pi^3\left(\frac{\ln(1/\phi)}{\ln^2(\kappa^{1/2}/a)}\right)\right.$$
$$\left.+\frac{2\sqrt{11}}{3}\pi^2\left(\frac{\ln(1/\phi)}{\ln^2(\kappa^{1/2}/a)}\right)^2(0.30\ldots)\right]\delta_{j3}\,\delta_{k3}(\delta_{kn}-\delta_{k3}\,\delta_{n3})$$
$$+\left(\frac{De}{4\pi^2}\right)\left[\sqrt{\frac{11}{27}}\frac{\pi^2}{2}\left(\frac{\ln(1/\phi)}{\ln^2(\kappa^{1/2}/a)}\right)^2(0.11\ldots)\right](\delta_{j1}\,\delta_{k2}\,\delta_{m1}\,\delta_{n2}+\delta_{j2}\,\delta_{k1}\,\delta_{m2}\,\delta_{n1}). \quad \text{(A 17)}$$

REFERENCES

BIRD, R. B., CURTISS, C. F., ARMSTRONG, R. C. & HASSAGER, O. 1978 *Dynamics of Polymeric Liquids: Volume 2. Kinetic Theory.* John Wiley and Sons.

BRANDRUP, J. & IMMERGUT, E. H. 1989 *Polymer Handbook.* Wiley Interscience.

CATHEY, C. A. & FULLER, G. G. 1990 The optical and mechanical response of flexible polymer solutions to extensional flow. *J. Non-Newtonian Fluid Mech.* **34**, 63.

CHILCOTT, M. D. & RALLISON, J. M. 1988 Creeping flow of dilute polymer solutions past cylinders and spheres. *J. Non-Newtonian Fluid Mech.* **29**, 381.

CHIRINOS, M. L., CRAIN, P., LODGE, A. S., SCHRAG, J. L. & YARITZ, J. 1990 Measurements of N_1–N_2 and η in steady shear flow and η', η'', and birefringence in small-strain oscillatory shear for the polyisobutylene solution M1. *J. Non-Newtonian Fluid Mech.* **35**, 105.

CHMIELEWSKI, C., PETTY, C. A. & JAYARAMAN, K. 1990 Crossflow of elastic liquids through arrays of cylinders. *J. Non-Newtonian Fluid Mech.* **35**, 309.

COLEMAN, B. D., DILL, E. H. & TOUPIN, R. A. 1970 A phenomenological theory of streaming birefringence. *Arch. Rat. Mech. Anal.* **39**, 358.

DEIBER, J. A. & SCHOWALTER, W. R. 1979 Flow through tubes with sinusoidal axial variations in diameter. *AIChE J.* **25**, 638.

DOI, M. & EDWARDS, S. F. 1986 *The Theory of Polymer Dynamics.* Oxford Science Publications.

DUPUIS, D., LAYEC, Y. & WOLFF, C. 1986 Rheo-Optical Properties of Polymer Solutions. In *Optical Properties of Polymers* (ed. G. H. Meeten). Elsevier.

DURST, F., HAAS, R. & KACZMAR, B. U. 1981 Flows of dilute hydrolyzed polyacrylamide solutions in porous media under various solvent conditions. *J. Appl. Polymer Sci.* **26**, 3125.

FLORY, P. J. 1953 *Principles of Polymer Chemistry.* Cornell University Press.

FRATTINI, P. L. & FULLER, G. G. 1984 A note on phase-modulated flow birefringence. A promising rheo-optical method. *J. Rheol.* **28**, 61.

FRATTINI, P. L., SHAQFEH, E. S. G., LEVY, J. L. & KOCH, D. L. 1991 Observations of axisymmetric tracer particle orientation during flow through a dilute fixed bed of fibers. *Phys. Fluids* A **3**, 2516.

FULLER, G. G. 1990 Optical rheometry. *Ann. Rev. Fluid Mech.* **22**, 387.

FULLER, G. G. & LEAL, L. G. 1980 Flow birefringence of dilute polymer solutions in two-dimensional flows. *Rheol. Acta* **19**, 580.

GALANTE, S. R. 1991 An investigation of planar entry flow using a high resolution flow birefringence method. PhD thesis, Carnegie Mellon University.

GALANTE, S. R. & FRATTINI, P. L. 1993 Spatially resolved birefringence studies of planar entry flow. *J. Non-Newtonian Fluid Mech.* **47**, 289.

GEFFROY, E. & LEAL, L. G. 1990 Flow birefringence studies in transient flows of a two-roll mill for the test-fluid M1. *J. Non-Newtonian Fluid Mech.* **35**, 361.

GENNES, P. G. DE 1979 *Scaling Concepts in Polymer Physics.* Cornell University Press.

HARLEN, O. G., HINCH, E. J. & RALLISON, J. M. 1992 Birefringent pipes: The steady flow of a dilute polymer solution near a stagnation point. *J. Non-Newtonian Fluid Mech.* **44**, 229.

HINCH, E. J. 1977 An averaged-equation approach to particle interactions in a fluid suspension. *J. Fluid Mech.* **83**, 695.

JACKSON, G. W. & JAMES, D. F. 1986 The permeability of fibrous porous media. *Can. J. Chem. Engng* **64**, 364.

JAMES, D. F. & MCLAREN, D. R. 1975 The laminar flow of dilute polymer solutions through porous media. *J. Fluid Mech.* **70**, 733.

JANESCHITZ-KREIGL, H. 1983 *Polymer Melt Rheology and Flow Birefringence.* Springer.

KISHBAUGH, A. J. & MCHUGH, A. J. 1993 A rheo-optical study of shear-thickening and structure formation in polymer solutions. *Rheo. Acta.* **32**, 9.

KUHN, W. & GRUN, F. 1942 Relationships between elastic constants and stretching double refraction of highly elastic substances. *Kolloid Z.* **101**, 248.

LARSON, R. G. 1988 *Constitutive Equations for Polymer Melts and Solutions.* Butterworths.

LARSON, R. G., KHAN, S. A. & RAJU, V. R. 1988 Relaxation of stress and birefringence in polymers of high molecular weight. *J. Rheol.* **32**, 145.

MARSHALL, R. J. & METZNER, A. B. 1967 Flow of viscoelastic fluids through porous media. *Ind. Eng. Chem. Fundam.* **6**, 393.

MCHUGH, A. J., MACKAY, M. E. & KHOMAMI, B. 1988 Measurement of birefringence by the method of isoclines. *J. Rheol.* **31**, 619.

MCKINLEY, G. H., ARMSTRONG, R. C. & BROWN, R. A. 1993 The wake instability in viscoelastic flow past confined circular cylinders. *Phil. Trans. R. Soc. Lond.* A **344**, 1.

MENASVETA, M. J. & HOAGLAND, D. A. 1991 Light scattering from dilute poly(styrene) solutions in uniaxial elongational flow. *Macromolecules* **24**, 3427.

MULLER, A. J., ODELL, J. A. & TATHAM, J. P. 1990 Stagnation-point extensional flow behavior of M1. *J. Non-Newtonian Fluid Mech.* **35**, 231.

NG, R. C.-Y. & LEAL, L. G. 1993 Concentration effects on birefringence and flow modification of semidilute polymer solutions in extensional flows. *J. Rheol.* **37**, 443.

NGUYEN, D. A. & SRIDHAR, T. 1990 Preparation and some properties of M1 and its constituents. *J. Non-Newtonian Fluid Mech.* **35**, 93.

OLBRICHT, W. L., RALLISON, J. M. & LEAL, L. G. 1982 Strong flow criteria based on microstructure deformation. *J. Non-Newtonian Fluid Mech.* **10**, 291.

PEARSON, D. S., KISS, A. D., FETTERS, L. J. & DOI, M. 1989 Flow-induced birefringence of concentrated poly-isoprene solutions. *J. Rheol.* **33**, 517.

PETERLIN, A. 1961 Streaming birefringence of soft linear macromolecules with finite chain length. *Polymer* **2**, 257.

PETERLIN, A. 1976 Optical effects in flow. *Ann. Rev. Fluid Mech.* **8**, 35.

PHILLIPPOFF, W. 1964 Streaming birefringence of polymer solutions. *J. Polymer Sci.* **5**, 1.

PILITSIS, S. & BERIS, A. N. 1989 Calculations of steady-state viscoelastic flow in an undulating tube. *J. Non-Newtonian Fluid Mech.* **31**, 231.

QUINZANI, G. H., MCKINLEY, G. H., BROWN, R. A. & ARMSTRONG, R. C. 1990 Modeling the rheology of polyisobutylene solutions. *J. Rheol.* **34**, 705.

SHAQFEH, E. S. G. & KOCH, D. L. 1990 Orientational dispersion of fibers in extensional flows. *Phys. Fluids* A **2**, 1077.

SHAQFEH, E. S. G. & KOCH, D. L. 1992 Polymer stretch in dilute fixed beds of fibres or spheres. *J. Fluid Mech.* **244**, 17.

SKARTSIS, L., KHOMAMI, B. & KARDOS, J. L. 1992 Polymeric flow through fibrous media. *J. Rheol.* **36**, 589.

SRIDHAR, T. 1990 An overview of the project M1. *J. Non-Newtonian Fluid Mech.* **35**, 85.

TANNER, R. I. 1985 *Engineering Rheology.* Oxford Science Publications.

TOWNSEND, P. 1980 A numerical simulation of Newtonian and viscoelastic flow past stationary and rotating cylinders. *J. Non-Newtonian Fluid Mech.* **6**, 219.

WALES, J. L. S. 1976 *The Application of Flow Birefringence to Rheological Studies of Polymer Melts.* Delft University Press.

ZICK, A. A. & HOMSY, G. M. 1984 Numerical simulation of the flow of an Oldroyd fluid through a periodically constricted tube. *Proc. IX Intl Cong. on Rheology*, p. 663.